Final Draft
of the original manuscript:

Ruckdaeschel, H.; Sandler, J.K.W.; Altstaedt, V.; Schmalz, H.; Abetz, V.; Mueller, A.H.E.:

Toughening of immiscible PPE/SAN blends by triblock terpolymers

In: Polymer (2007) Elsevier

DOI: 10.1016/j.polymer.2007.03.005

Toughening of immiscible PPE/SAN blends by triblock terpolymers

***Holger Ruckdäschel*[a], *Jan K.W. Sandler*[a], *Volker Altstädt*[a,*], *Holger Schmalz*[b] *Volker Abetz*[b,#] *and Axel H.E. Müller*[b,*]**

(a) Polymer Engineering, University of Bayreuth, D-95440 Bayreuth, Germany

(b) Macromolecular Chemistry II, University of Bayreuth, D-95440 Bayreuth, Germany

ABSTRACT

The mechanical performance of immiscible blends of poly(2,6-dimethyl-1,4-phenylene ether) (PPE) and poly(styrene-*co*-acrylonitrile) (SAN) and the subsequent influence of compatibilisation by tailored polystyrene-*block*-polybutadiene-*block*-poly(methyl methacrylate) triblock terpolymers (SBM) on the mechanical performance under static and dynamic loads is analysed in detail. A PPE/SAN 60/40 blend was selected as a base system for the compatibilisation experiments. The observed static tensile behaviour is described by micromechanical models and correlated to the blend microstructures as observed by transmission electron microscopy. In most cases, the addition of the SBM triblock terpolymers further enhances the ductility of the blend while only leading to a minor reduction of modulus and strength. Triblock terpolymers with symmetric end blocks, mainly located at the interface between PPE and SAN, led to nearly isotropic specimens. In contrast, SBM materials with a longer polystyrene block predominantly formed micelles in the PPE phase and the blends revealed a highly anisotropic morphology. Comparative investigations of the fatigue crack growth behaviour parallel to the direction of injection also reflected this variation in mechanical anisotropy of the compatibilised blends. A poor toughness and a predominant interfacial failure were observed in the case of the SBM with a long polystyrene block. In contrast, a considerable improvement in properties as a result of pronounced plastic deformations was observed for blends compatibilised by triblock terpolymers with symmetric end blocks. The systematic correlation between morphology and mechanical performance of compatibilised PPE/SAN blends established in this study provides an efficient way for the desired selection of suitable and effective compatibilising agents, ensuring both a superior multiaxial toughness as well as a high strength and modulus of the overall system.

(Keywords: polymer blend, compatibilisation, triblock terpolymer, mechanical properties)

* To whom correspondence should be addressed:

Volker Altstädt, Email: altstaedt@uni-bayreuth.de, Tel. +49-921-55-7470, Fax: +49-921-55-7473

Axel H.E. Müller, Email: axel.mueller@uni-bayreuth.de, +49-921-55-3399, Fax: +49-921-55-3393

Present address: Institute of Polymer Research, GKSS Research Centre Geesthacht, D-21502 Geesthacht, Germany

1 INTRODUCTION

Blending of polymers is as a beneficial approach towards providing materials with a set of desired properties [1,2]. In particular, two-phase blends consisting of at least two components are often favoured, as an exploitation of the advantageous properties of each component appears feasible [1]. For example, binary blends of poly(2,6-dimethyl-1,4-phenylene ether) (PPE) and poly(styrene-*co*-acrylonitrile) (SAN) have been identified as a promising system due to the possible combination of the high heat distortion temperature and toughness of the PPE with the desirable properties of SAN such as the chemical resistance, good processability as well as low material cost [3,4]. However, the interfacial adhesion of such two-phase blends is often limited as a result of the incompatibility between the blend components, leading to a subsequent degradation of the mechanical performance and brittle characteristics. In case of binary PPE/SAN blends, Merfeld et al. [5] reported a strongly segregated behaviour and an interfacial thickness of only 5 nm (for an acrylonitrile content of 20 wt% in SAN). Consequently, a poor fracture toughness and ultimate fracture strain less than the linear rule-of-mixture expectations can be anticipated.

In fact, such a behaviour has been verified by earlier studies investigating PPE/SAN 40/60 and PPE/ABS 48/52 blends, respectively, revealing a brittle mechanical response for blends prepared by solvent-mediated as well as by melt-processing approaches [3-7]. Nevertheless, Fekete et al. [8] recently reported contrary results for melt-blended PPE/SAN: over a wide compositional range, a reasonable agreement between experimental data regarding the modulus and strength and theoretical predictions based on a linear rule-of-mixture approach were shown. However, as both the blend morphology and the acrylonitrile content,- two key parameters determining the mechanical properties of such blends - were neglected in these studies, a systematic investigation of the influence of these parameters on the deformation behaviour is needed. In addition, the demand for a further enhancement of the mechanical properties of such PPE/SAN blends remains.

In general, compatibilisation is an efficient and well-accepted method to improve the interfacial strength between the components in a two-phase blend [1,2,9]. In addition, the interfacial tension and the coalescence between the blend partners is decreased, effects that lead to a finer morphology [10], which also is beneficial for the overall mechanical performance [11]. Block copolymers, in particular, are commonly used to improve the adhesion of immiscible blend components due to a selective miscibility of the blocks with either blend component [12-15]. In the case of PPE/SAN blends, polystyrene-*block*-poly(methyl methacrylate)

diblock copolymers (PS-*b*-PMMA, SM) are very suitable to act as a compatibiliser due to the favourable enthalpic interaction between PS and PPE as well as between PMMA and SAN, respectively [4,16,17]. It has been demonstrated that the interfacial toughness, as determined by dual cantilever beam tests, can be significantly increased by such a compatibilisation step [18]. Furthermore, Stadler et al. [16,17] reported a notable reduction of the domain size of PPE/SAN blends by the addition of such copolymers. However, the overall mechanical toughness of these blends remained unsatisfactorily low [3,4].

Thermal stresses at the interface between PPE and SAN occurring as a result of the different thermal coefficients of expansion during solidification following melt-processing were identified as a crucial reason for the observed brittle behaviour [3]. In order to overcome the build-up of these stresses, the addition of triblock terpolymers as compatibilising agents with an elastomeric middle block and end blocks of PS and PMMA, respectively, appears advantageous. Again, Stadler et al. developed this concept; investigating morphological as well as thermal and mechanical features of solution-precipitated and hot-pressed ternary PPE/SAN/triblock terpolymer blends [3], using polystyrene-*block*-poly(ethylene-co-butylene)-*block*-poly(methyl methacrylate) (SEBM) as a compatibiliser. As a result of the particular thermodynamic interaction between the relevant blocks and the blend components, a discontinuous distribution of the elastomer at the interface, the so-called "raspberry morphology", was observed (Fig. 1). The mechanical characterisation revealed a significant ductility improvement for these SEBM-compatibilised blends as compared to both the uncompatibilised as well as the SM-compatibilised PPE/SAN blends [3,4]. In addition, it is this discontinuous interfacial coverage by the elastomer as compared to a continuous poly(ethylene-co-butylene) (PEB) layer which minimises the loss in modulus. However, as the chosen testing procedure differs from standardised techniques such as tensile testing, the significance of the presented mechanical data is, as yet, limited.

Lach et al. [6] as well as Kirschnick et al. [7] reported first approaches towards the melt-processing of PPE/SAN blends compatibilised by similar triblock terpolymers, more precisely polystyrene-*block*-polybutadiene-*block*-poly(methyl methacrylate) (SBM). Nevertheless, only Lach et al. [6] evaluated the resulting impact behaviour of the compatibilised blends by characterising the resistance to unstable crack initiation under dynamic loading conditions and by employing elastic-plastic fracture mechanics (EPFM). Again, an increasing toughness of the system with an increasing SBM content and, finally, stable crack growth at rubber contents of 15 wt% were observed while the calculated blend modulus remained at a reasonably constant level. However, only limited information was provided regarding the deformation mecha-

nism; the authors postulated that the high toughness is a result of interfacial cavitation, stretching of the elastomer, and subsequent shear deformation of the SAN matrix due to the stress concentration.

In order to further evaluate the micromechanical effect of SBM addition on PPE/SAN blends, Brown et al. characterised the interfacial properties of selected blends by the dual cantilever beam approach [18] using SBM materials with symmetric end blocks and varying lengths of the elastomeric PB middle block. Such a characterisation technique is well accepted to investigate the interfacial toughness of a blend as a function of the interfacial thickness and, thus, provides valuable information regarding the deformation mechanism of multiphase blends. Surprisingly, the addition of SBM led to an interfacial toughness which decreased below the level of the uncompatibilised system at low interfacial thicknesses [18]. At an elevated interfacial thickness of approximately 40 nm, the toughness increased again, eventually exceeding the value of the neat PPE/SAN interface. Yet, a direct comparison revealed a significantly enhanced performance when using SM diblock copolymers. The presence of the elastomeric middle block at the interface was proposed as the main reason for the low interfacial toughness of the SBM compatibilised systems, as the elastomer suppresses crazing due to the limited load transfer and leads to failure by deformation mechanisms such as slow disentanglement as well as chain scission.

In summary, an enhanced toughness of immiscible PPE/SAN blends due to the addition of suitable triblock terpolymers has been verified; however, a more detailed investigation of the morphological phenomena related to the elastic as well as inelastic deformation behaviour of such PPE/SAN/SBM blends is desirable. The aim of this study, therefore, was to establish a systematic correlation between the blend morphology, the static mechanical and the fatigue crack growth behaviour of uncompatibilised as well as compatibilised PPE/SAN blends prepared by twin-screw extrusion and subsequent injection-moulding. The PPE/SAN ratio of the uncompatibilised blends was varied between 20 and 60 wt% of PPE. All compatibilised blends, however, were prepared at a constant PPE/SAN ratio of 60/40. Four SBM triblock terpolymers with varying compositions were used with weight fractions of up to 20 wt%.

2 EXPERIMENTAL

2.1 Materials and compositions

The commercial poly(styrene-*co*-acrylonitrile) resin (SAN, grade VLL 19100, BASF AG, Ludwigshafen, Germany) used in this study is a copolymer with an acrylonitrile content of

19 wt%, a weight-average molecular weight of M_w = 112 kg/mol, and a polydispersity index of 1.95. This comparatively low acrylonitrile content ensures homogeneous miscibility between SAN and PMMA at the relevant processing conditions [20]. In contrast to the SAN in pellet form, non-commercial poly(2,6-dimethyl-1,4-phenylene ether) (PPE, grade PX100F, Mitsubishi Engineering Plastics Europe, Düsseldorf, Germany) was obtained as a powder, with a weight-average molecular weight of M_w = 12.9 kg/mol, and a polydispersity of 1.63. It should be noted that PPE is also frequently referred to as PPO (poly(2,6-dimethyl-1,4-phenylene oxide)), especially in the American-Pacific region. The average molecular weights of both SAN and PPE were determined by GPC analysis using an UV detector relative to polystyrene standards at 40 °C, with THF as a solvent. Irganox 1010 and Irgafos 168 (Ciba AG) were used as stabilisers. Irganox 1010 is a sterically hindered phenol and acts as chain-breaking antioxidant by rapidly reacting with peroxy radicals (ROO·) to break the cycle. Irgafos 168, as a secondary antioxidant, reacts with hydroperoxides (ROOH) to yield non-radical, non-reactive products. Such secondary antioxidants are particularly effective in a synergistic combination with primary antioxidants, as applied in the present study.

Different SBM triblock terpolymers with varying block lengths and a narrow molecular weight distribution were synthesised by sequential anionic polymerisation as described previously [19]. The molecular properties of the triblock terpolymers are summarised in Table 1. All molecular weights of the SBM materials were carefully selected to be equal to or above the critical molecular mass for entanglement (critical molecular mass of 31.2 kg/mol of polystyrene and 18.4 kg/mol of poly(methyl methacrylate), respectively [21]). With regard to SBM1, SBM2 and SBM3, the weight ratio between polybutadiene and poly(methyl methacrylate) was kept almost constant, whereas the weight content of polystyrene is adjusted to be either lower, equal to or higher than the other blocks, respectively. In SBM4, the weight fraction of the end blocks is balanced; here, the amount of the polybutadiene middle block is reduced. Following the synthesis, the SBM were cryo-ground in order to enable a homogenous distribution of the SBM in the dry-blends with PPE and SAN.

2.2 Melt processing of the blends – extrusion and injection-moulding

Prior to the melt-blending operations, the PPE powder and the SAN pellets were vacuum-dried at 80 °C for 12 hours. In contrast, the SBM terpolymers were dried at 40 °C. Subsequently, PPE, SAN, and SBM were dry-blended using metered weight contents of the SBM compatibiliser. Initially, uncompatibilised PPE/SAN blends with PPE weight fractions between 20 and 60 wt% were prepared. For all compatibilised systems, the ratio of PPE to SAN

was kept constant at 60/40 and the weight contents of the SBM were set at 0, 5, 10 and 20 wt%, respectively (Table 2). Furthermore, 0.1 wt% of stabiliser (mixture of 2 parts Irganox 1010 and 1 part Irgafos 168) was added to prevent thermal degradation, especially cross-linking of PB and PPE. The final blend compositions are summarised in Table 2.

All materials were melt-blended using a co-rotating twin-screw extruder (Brabender DSE 20/40) with a screw diameter of 20 mm and a screw length of 600 mm (L/D = 30). The maximum barrel temperature and the nozzle temperature were set at 250 °C and 245 °C, respectively. The throughput was kept constant at 1.3 kg/h using a constant screw speed of 50 rpm by volumetric feeding. The screw set-up as well as the processing parameters were established in preliminary investigations and were carefully selected in order to minimise degradation while allowing a sufficient mixing time and efficiency. In the present study, the screw set-up consisted of two distinct kneading zones made up of various kneading blocks and a back-pumping element each. Consequently, the mean residence time of all blends in the extruder was approximately 5 min. The melt strands were subsequently quenched in water and were chopped into pellets.

Detailed rheological tests prior to the melt-processing as well as subsequent size exclusion chromatographic analysis of the materials revealed rather constant rheological properties for the selected processing times and the molecular weight distributions following melt-compounding were similar to those of the non-processed materials. Although the experimental data and discussion are omitted, it should be noted that both approaches thus verified the minimised thermal and shear degradation under the chosen processing conditions.

Tensile test specimens according to ISO 527-2 (thickness 2 mm, width 4 mm) as well as rectangular plates (70 mm x 70 mm x 4 mm) were prepared by injection-moulding using an Arburg Allrounder 320S 500-150 (screw diameter of 30 mm) at an injection speed of 114 cm^3/s. The maximum barrel temperature was set at 280 °C. The mould temperature was limited to 80 °C in order to guarantee demoulding without deforming the specimens. It must be noted that neat PPE reference specimens were prepared by hot-pressing at 250 °C as the limited thermal stability prevented injection-moulding.

2.3 Morphological investigations

Ultra-thin sections (50 nm) of the injection-moulded tensile test specimens were cut at room temperature using an ultra-microtome (Reichert-Jung Ultracut E microtome) and a diamond knife. The sections were subsequently stained using OsO_4 and RuO_4 following an established procedure [3,7,19]. Due to this particular staining method, SAN and PPE appear as the bright

and dark phase, respectively, whereas the PB block of the SBM appears black [19]. Bright-field transmission electron microscopy (TEM) was carried out using a Zeiss 902 TEM operating at an acceleration voltage of 80 kV.

2.4 Mechanical testing

All tensile properties were measured according to ISO 527 at 23 °C and 50 % relative humidity using a Zwick 1445 universal testing machine. A minimum number of five specimens was used for each individual material composition and the average values are reported. The Young's modulus (tensile modulus) was determined at a crosshead speed of 1 mm/min. Reaching a sample deformation of 0.25 %, the crosshead speed was increased to 5 mm/min and was kept constant until fracture of the specimens occurred.

Fatigue crack propagation (FCP) tests were performed at 23 °C and 50 % relative humidity, employing a computer-controlled, servo-hydraulic test machine (Schenck MHF, IST 8400), a sinusoidal waveform and a cyclic frequency of 10 Hz. The used compact tension (CT) specimens were machined out of the injection-moulded rectangular plates. Razor-blade tapping was used to introduce a sharp crack at the notch-tip just before the start of the experiment. The specimens were loaded for crack propagation either in perpendicular or in parallel to the injection-direction (melt-flow direction). The compliance of the specimen was continuously measured by the crack opening displacement method using a transducer fixed to the front face of the CT-specimen with rubber bands. The ratio of the minimum to the maximum stress, the so-called R-ratio, was set at 0.1, the stress intensity factors were calculated according to [22]. The FCP tests were performed at increasing stress intensity factors (ΔK) with a constant ΔK gradient as a function of the crack length a of 0.15 mm^{-1}. A detailed description of this particular FCP procedure is given in [22, 23].

2.5 Investigation of the fracture surfaces

The specimen fracture surfaces obtained by the FCP tests were first coated with a thin layer (2 nm) of platinum and were subsequently analysed using a field emission scanning electron microscope (Zeiss 1530 FESEM) operating at an acceleration voltage of 2 kV. Micrographs were taken using the In-Lens secondary electron (SE) detector in order to evaluate the surface topography.

3 RESULTS AND DISCUSSION

3.1 Tensile properties of immiscible PPE/SAN blends

The mechanical properties of immiscible blends in general strongly depend on the phase content, the resulting morphology as well as on the mechanical behaviour of the individual components [1,2]. In addition, the interfacial adhesion has been identified as a key parameter determining the material characteristics such as toughness and strength observed at larger strains [1,2,24]. A detailed investigation of the mechanical performance of uncompatibilised PPE/SAN blends therefore not only allows a target-oriented selection of the blend composition for the following compatibilisation step using SBM triblock terpolymers but also provides a detailed insight into the phase morphology and interfacial properties of PPE/SAN blends.

3.1.1 Elastic properties of PPE/SAN blends (low-strain behaviour)

For the evaluation of the tensile modulus typically analysed at very low strains, the adhesion between the two blend phases can be regarded as sufficiently high to ensure load transfer between PPE and SAN [25,26]. Based on this assumption, the well-known parallel and series models (Eq. 1 and 2, respectively) can be considered as first approximations of the upper and lower bounds of the modulus of two-phase PPE/SAN blends:

$$E_{blend} = \phi_{PPE} E_{PPE} + \phi_{SAN} E_{SAN}, \qquad (1)$$

$$\frac{1}{E_{blend}} = \frac{\phi_{PPE}}{E_{PPE}} + \frac{\phi_{SAN}}{E_{SAN}}, \qquad (2)$$

where E and ϕ denote the tensile modulus and the phase content, respectively. The indices PPE, SAN, and blend denote the particular phase as well as the blend, respectively. It should be noted that the volume content of each phase is similar to the weight content (Table 2), as the density of PPE (1.065 g/cm^3) and SAN (1.07 g/cm^3) are nearly identical.

As the tensile moduli of neat PPE (2.5 GPa) and of neat SAN (3.8 GPa) are rather similar, both models lead to predictions with relatively little difference; for a PPE/SAN 50/50 blend, for example, an upper bound of 3.15 GPa (Eq. 1) and a lower bound of 3.02 GPa (Eq. 2) are predicted. Hence, utilisation of more complex theoretical approaches such as coupling models [27] and self-consistent models [28, 29] leading to more precise values does not appear necessary.

All relevant mechanical properties of the PPE/SAN blends following injection-moulding observed by tensile testing are summarised in Tab. 3. As shown in Fig. 2, the tensile modulus of PPE/SAN blends as a function of the blend composition follows the upper bound prediction in the compositional range between 40 to 60 wt% of PPE. In contrast, a PPE content of 20 wt% leads to a deviation from this predicted linear relationship, the experimental value is closer to the lower bound prediction in this specific case. Considering the selected compositional range, the SAN forms the continuous phase in all blends. The PPE, however, is fully dispersed at low PPE contents (20 wt%) only and shows some continuity at higher PPE contents (60 wt%). The evolution of such morphological features has been discussed previously, e.g. by taking into account the viscosity ratio [19]. As PPE contents above 60 wt% necessitate further increased processing temperatures exceeding the thermal stability of both neat PPE and SAN, and, in particular, of the SBM for the subsequent compatibilisation step [19], such blend compositions were not prepared.

In order to correlate the elastic behaviour of the blends to the phase morphology, TEM micrographs of the PPE/SAN 60/40 blend were taken both parallel as well as normal to the injection direction. The skin and core region of the parallel section of the tensile bar were analysed separately. The TEM micrographs shown in Fig. 3 highlight the continuous structure of the SAN phase (bright), whereas the PPE forms rather complex and deformed particles. The PPE phase does not appear fully dispersed but shows a remarkable degree of continuity, as demonstrated by the connectivity between the individual particles (Fig. 3a and 3c) [19]. Furthermore, the observed morphologies reveal a significant degree of orientation; the PPE phase is highly elongated in the direction of the flow. This effect can particularly be seen in the skin region showing a fibre-like appearance (Fig. 3d). In the core region, the PPE phase is less deformed as a result of the lower shear forces and an increased time span to relax during the injection-moulding process (Fig. 3 b) [30]. Such a layered skin-core morphology is typical for injection-moulded two-phase blends [1, 26,30-32].

This pronounced degree of orientation of the dispersed PPE phase in the PPE/SAN 60/40 blend explains the good agreement of the experimental values with the predictions based on the parallel model (Eq. 1). A reduction of the PPE content leads to a decreasing anisotropy of the PPE phase, and the mechanical properties of the blends are subsequently determined by a combination of both the parallel and the series model.

3.1.2 Inelastic properties of PPE/SAN blends (high-strain behaviour)

Similar to the materials response at low strains, the mechanical behaviour of blends at elevated stress and strain levels is strongly dependent on the blend composition and on the phase morphology. In addition, the mechanical compatibility, the interfacial adhesion as well as the phase size of the two-phase blend become more important and, finally, determine the ultimate strength, the ductility, and the toughness of such systems.

Most theoretical considerations focus on complex calculation methods to predict the tensile strength of blends; yet again, the well-known series and parallel model are frequently used (Eq. 3 and 4). In case of the parallel model, it should be noted that the material fails as soon as the stress of the phase with the lower tensile strength is reached:

$$\sigma_{blend} = \phi_{PPE}\sigma_{PPE} + \phi_{SAN}\sigma_{SAN}, \qquad (3)$$

$$\sigma_{blend} = \min(\sigma_{PPE}, \sigma_{SAN}) = \sigma_{PPE}, \qquad (4)$$

where σ denotes the tensile strength of the material. However, perfect phase adhesion and, thus, complete load transfer between the two phases is assumed [33]. In contrast to the low-strain regime, such a perfect phase adhesion cannot be expected for all blend systems at elevated strain levels beyond the limit of linearity in priori.

Both the experimentally observed tensile strength data as well as the theoretical predictions according to Eq. 3 and 4 are summarised in Fig. 4a. As the materials showed either yielding or a brittle fracture depending on the blend composition, the abbreviations ‘Y’ and ‘B’ respectively are introduced in order to highlight the respective deformation mechanism. For each material, the maximum stress is reported (yield strength or strength at break, respectively). As can be seen, neat SAN as well as blends with PPE contents below 60 wt% reveal brittle characteristics, whereas PPE/SAN 60/40 as well as neat PPE show a pronounced yielding before failure.

The tensile strength of the PPE/SAN 50/50 and 60/40 blends is in reasonable agreement with the model given by Eq. 3, reflecting the particular phase morphology as already discussed for the elastic behaviour as well as a significant degree of interfacial adhesion. Similar results were observed by Fekete et al. [8] for PPE/SAN blends over the whole composition range. In contrast to this trend, the tensile strength data shown here deviate from the linear relationship for a PPE content of 20 wt%, and is even slightly below predictions based on Eq. 4. This de-

viation is related to the change in blend morphology as well as to a partial debonding in the interfacial region, more specifically at the interfaces normal to the direction of the tensile load, for this particular composition.

The strain at break and the yield strain (for materials showing yielding) are summarised in Fig. 4b. The dashed line represents a prediction of the blend behaviour based on a linear relationship between the strain at break of SAN and the yield strain of PPE, respectively:

$$\varepsilon_{blend}\Big|_{\sigma_{\max}} = (\phi_{PPE}\varepsilon_{yield,PPE} + \phi_{SAN}\varepsilon_{break,SAN}). \qquad (5)$$

As discussed before, the brittle-to-tough transition for blend compositions containing at least 60 wt% of PPE is seen again, indicated by relatively high elongations at break (exceeding 40 % for PPE/SAN 60/40). It is worth noting that the yield strain of this PPE/SAN 60/40 blend perfectly matches the linear prediction (Eq. 5) and, moreover, that the elongation at break follows the same additivity rule; promoting the conclusion of mechanical compatibility between both blend phases. At lower contents of PPE, however, all materials behave in a brittle manner and show a negative deviation from the prediction. The elongation at break of the PPE/SAN 20/80 blend is even below that of the neat SAN, reflecting a premature failure of the SAN matrix as a result of the dispersed PPE phase. Similar general trends have been reported for blends of PC/SAN and PC/ABS, where a sufficient fraction of the more ductile PC is essential in order to achieve a high blend toughness [34-37].

3.1.3 Deformation mechanism of PPE/SAN blends (micromechanics)

This general mechanical property profile, the tough behaviour of the binary PPE/SAN 60/40 blend particularly, implies that the macroscopically brittle SAN phase can show a ductile behaviour on the microscopic scale as the high elongation at break of the 60/40 blend cannot be related to the ductile PPE phase alone. Such a brittle-to-ductile transition of SAN has been reported in several studies and is assigned to diverse factors including the multiaxial state of stress within the SAN phase [25], a relatively small dispersed blend phase size [32], a significant degree of continuity of the second (ductile) blend phase [34-37], and/or a layer-like structure of the ductile phase [38].

With regard to the multiaxial state of stress, it has been stated [35,36] that brittle thermoplastic phases can undergo plastic deformation if the following requirements are fulfilled: (1) the brittle phase is dispersed in a ductile matrix; (2) the compressive stresses evolving by the bulk deformation of the two-phase polymer blend as a result of the difference in elastic properties (tensile modulus, Poisson's ratio) exceed a certain critical value; (3) the load transfer between

the two phases is sufficient to induce deformation. These deformation phenomena, also known as the "cold-drawing concept", have been demonstrated for various blends [35,36,39]. In the case of PPE/SAN, both the second as well as the third requirement are fulfilled. The compressive stresses predicted by the equations of Takayashi et al. [40] are about 8.4 MPa at a deformation of 4% (tensile moduli of 2.5 GPa (PPE) and 3.8 GPa (SAN), Poisson's ratios of 0.4 (PPE) and 0.35 (SAN) as taken from the experimental data and literature values, respectively) and, thus, approach the compressive strength of SAN of around 9 MPa [36].

However, the first requirement is not satisfied for the present PPE/SAN 60/40 blend as SAN tends to form the continuous phase within the blend. Nevertheless, Kolarik et al. [25] demonstrated for PC/SAN blends that the stress conditions for plastic microdeformation of the macroscopically brittle SAN embedded in a ductile PC matrix are not as strict as stated above [35,36]. The cold-drawing phenomenon was also observed for systems where the PC showed a sufficient degree of continuity within a continuous SAN phase. The corresponding morphologies for PC/SAN 50/50 blends [25] are similar to the ones observed here for the PPE/SAN 60/40 blend revealing a macroscopically tough behaviour and yielding of the SAN phase.

The deformation and yielding behaviour of well-defined multi-layered blends was extensively analysed as a function of the blend partners and of the interlayer thickness [41-43]. In all cases, the interfacial strength becomes more important as the interlayer thickness increases, and as sufficiently high stress transfer between the two phases on a macroscopic scale is ensured for low ligament thicknesses, e.g. between PE and PPE/PS [42]. Similar results of cooperative yielding of multi-layers were observed for PC/SAN [41]. For example, microcracking of the SAN induces local delaminations at the PC/SAN interface if the adhesion is sufficiently low. Consequently, the PC layers are allowed to draw out and, thus, improve the toughness of the multi-layer. Similarly, the evolution of crazes and cracks in SAN and the subsequent initiation of shear bands in the PC were reported by Gregory et al. [43].

Returning to the PPE/SAN blends, the morphological features of the 60/40 blend composition as shown in Fig. 3 resemble a structure similar to multi-layers of PPE and SAN. Nevertheless, the unknown extent of the interfacial adhesion necessitates further consideration. For an acrylonitrile content of 20 wt% in SAN - similar to the one used in this study - an interfacial thickness of only 5 nm has been observed for a PPE/SAN system [5]. Yet, a similar interfacial thickness of about 5 nm for PC/SAN blends [1] and the corresponding load transfer in such

blends implies that there is a positive contribution of the interfacial adhesion in the case of PPE/SAN to the static tensile properties.

In summary, the cold-drawing mechanism, the fine phase morphology as well as the presence of oriented continuous PPE phases all appear to influence the deformation behaviour of the neat PPE/SAN blends. For the development of SBM-compatibilised PPE/SAN blends, the base composition of PPE/SAN 60/40 appears most promising as this particular blend combines a remarkably tough tensile behaviour, a satisfying processability, and enhanced thermo-mechanical properties as demonstrated earlier [19].

3.2 Tensile properties of PPE/SAN blends compatibilised by SBM

The addition of SBM triblock terpolymers can provide an efficient melt-compatibilisation of the immiscible PPE/SAN blend if both the SBM composition and the processing parameters are carefully selected. In the following section, the mechanical properties presented for the various compatibilised systems are correlated with the blend microstructures mainly, as a detailed overview of the blend nanostructures at the interfaces has been highlighted in a previous study [19]. As such, the relation 'compatibilisation efficiency' and the observed enhancement of the mechanical properties, which should not be equated in priori, will be addressed. As demonstrated, the addition of SBM triblock terpolymers with a nearly equal length of the end blocks such as SBM1, SBM2 and SBM4 led to an interfacial enrichment and, thus, to the desired melt-compatibilisation of the system. However, some micellation of these SBM types in the PPE phase was observed following the injection-moulding step. In contrast, SBM3 is located mostly in the PPE as a result of the high block length of PS.

3.2.1 Morphological features of PPE/SAN/SBM blends following injection-moulding

The mechanical behaviour of injection-moulded blends is influenced by the morphology of both the core as well as of the skin region of the specimens. In the case of the PPE/SAN 60/40 blend, there is a pronounced morphological difference between these two locations and, furthermore, strongly varying orientation effects were observed. In order to take these differences into account, TEM micrographs of all compatibilised PPE/SAN blends were taken both from the core and the skin region, both parallel as well as normal to the flow direction.

Fig. 5a-d highlights the morphology of injection-moulded blends compatibilised by 20 wt% of SBM2 as an example. As can be seen, the average phase size and the orientation effect are significantly reduced due to the compatibilisation as compared to the neat PPE/SAN 60/40 blend (Fig. 3), independent of position. Furthermore, there are small structural differences

between the core region (5a,b) and the skin region (5c,d) for this particular system. To some extent, the orientation of the PPE phase as indicated by the arrows in Fig. 5b and 5d remains visible. SAN still forms the continuous phase across the specimen, whereas the PPE appears not fully dispersed, indicating a significant degree of continuity. Similar results were observed for blends compatibilised by SBM1 and SBM4, respectively. In both of these cases, details regarding the differences in the microstructure such as micellation of the triblock terpolymer (SBM1) or an increased number of sub-inclusions in the PPE (SBM4) have been discussed previously [19].

Yet, the morphological features of PPE/SAN blends compatibilised by 20 wt% of SBM3 are significantly different (Fig. 5e-h). In this particular system, the core region shows a co-continuous character of PPE/SAN as a result of the enrichment of the SBM3 in the PPE phase [19]. Orientation effects are pronounced in the core and are also visible in the skin region (Fig. 5f,h). Furthermore, the PPE phase shows an increased tendency towards coalescence across the specimen, indicated by an increased average phase size (Fig. 5e-h). These effects lead to relatively large SAN-rich regions which are oriented parallel to the flow direction (Fig. 5f,h).

The mechanical properties of the PPE/SAN/SBM blends are summarised in Table 4. It is worth noting that all materials show yielding, except for the blend compatibilised by 5 wt% of SBM4. In order to establish a correlation between the mechanical behaviour and the SBM grade and content, respectively, the elastic properties will be discussed first.

3.2.2 Elastic properties of PPE/SAN/SBM blends (low-strain behaviour)

The tensile modulus of all compatibilised PPE/SAN blends as a function of the weight content of the SBM triblock terpolymers is shown in Fig. 6a. In general, addition of SBM leads to a reduction of the blend modulus. The content of the elastomeric middle block appears to be the main factor for this observed reduction. In order to further elucidate this effect, the modulus of the blends is evaluated as a function of the volume fraction of polybutadiene (Fig. 6b). The volume contents of the individual phases were calculated based on the density of the individual components (PPE 1.065 g/cm^3, SAN 1.07 g/cm^3, PS 1.05 g/cm^3, PB 0.9 g/cm^3, PMMA 1.19 g/cm^3) [44], respectively, and their respective weight contents by applying a linear rule-of-mixture approach. The dashed line in Fig. 6b represents a theoretical prediction based on a linear rule-of-mixture approach for the upper limit, calculated according to

$$E_{PPE/SAN/SBM} = (1-\phi_{PB})\, E_{PPE/SAN\,60/40} + \phi_{PB}\, E_{PB}, \qquad (6)$$

where $E_{PPE/SAN/SBM}$, $E_{PPE/SAN\,60/40}$, and E_{PB} denote the predicted modulus of the PPE/SAN/SBM blend, the experimentally observed modulus of the PPE/SAN 60/40 blend and the modulus of PB, respectively. ϕ_{PB} represents the volume content of the PB middle block in the blend. As the modulus of PB at ambient temperature is significantly lower than the modulus of the glassy phases, the contribution of the elastomeric middle block to the elastic blend properties can be neglected with regard to the linear rule-of-mixture approach.

A reasonable agreement between the experimental data and this simple theoretical prediction is observed within experimental accuracy up to PB contents of about 3 vol%, independent of SBM type. At higher PB volume contents, however, the elastic behaviour of the blends more strongly depends on the SBM grade used for the compatibilisation. On the one hand, the modulus of blends compatibilised by SBM3 remains at a relatively high level and is close to the upper-limit prediction. All blend systems compatibilised by SBM materials with (nearly) symmetric end blocks on the other hand show a substantial drop in modulus. This phenomenon is most pronounced for blends based on 20 wt% of SBM1 and SBM2, respectively.

These deviations especially reflect the microstructural differences of the blends as a function of the SBM type. In order to provide a more detailed description of the materials behaviour, the mechanical blend properties are calculated by taking into account the morphological features as obtained by the fundamental investigation presented in [19]. The comparison of the experimental modulus data shown for the blends compatibilised with SBM2 and SBM3 and the predictions of the more detailed models discussed below is presented in Fig. 7. For illustration purposes, schematic representations of the respective blend morphologies are included.

In the case of the SBM2 triblock terpolymer (Fig. 7a) with nearly equal block lengths of the PS and the PMMA blocks, respectively, a continuous interfacial enrichment of the block copolymer is observed. Using a simple approach and treating each component as an individual phase, the modulus $E_{PPE/SAN/SBM}$ of such a blend can be predicted by an additivity rule based on the moduli and the volume contents of the respective components:

$$E_{PPE/SAN/SBM} = \phi_{PPE}E_{PPE} + \phi_{SAN}E_{SAN} + \phi_{PS}E_{PS} + \phi_{PB}E_{PB} + \phi_{PMMA}E_{PMMA}. \qquad (7)$$

However, it should be noted that specific interactions between the block copolymer and the blend components, i.e. between PPE/PS and SAN/PMMA, respectively, are neglected. Although this simplification may be valid for the binary SAN/PMMA phase showing only weak interactions, the synergistic behaviour of PPE/PS blends often reported in the literature

[45,46] leads to a blend modulus well above the additivity prediction. These effects can be taken into account by the so-called Simplex equation, introducing the parameter $\beta_{PPE/PS}$ [45]:

$$E_{PPE/SAN/SBM} = \phi_{PPE}E_{PPE} + \phi_{PS}E_{PS} + \beta_{PPE/PS}\phi_{PPE}\phi_{PS} + \phi_{PB}E_{PB} + \phi_{SAN}E_{SAN} + \phi_{PMMA}E_{PMMA}. \quad (8a)$$

This value can be determined according to

$$\beta_{PPE/PS} = 4E_{PPE/PS(\phi_{PPE}=\phi_{PS}=0.5)} - 2E_{PPE} - 2E_{PS} \quad (8b)$$

using experimentally obtained moduli of PPE, PS and of a binary PPE/PS 50/50 blend, respectively. Although these systems are not discussed here, the following values were determined: $\beta_{PPE/PS}$=1.62 GPa, $E_{PPE/PS(\phi_{PPE}=\phi_{PS}=0.5)}$=3.32 GPa, and E_{PS}=3.33 GPa.

As shown in Fig. 7a, the Simplex prediction leads to a marginally higher blend modulus at higher SBM contents. Yet, the PPE/SAN blends compatibilised with SBM2 show a negative deviation from both theoretical predictions at higher SBM contents. This particular behaviour most likely is related to an increasing continuity of the interfacial coverage between PPE and SAN by the PB with increasing SBM content and, at some SBM content, the PB finally forms a fully continuous layer as shown schematically in Fig. 7a. Under the chosen processing parameters, this particular blend system reveals morphological characteristics showing both a discontinuous and continuous coverage [19].

The elastic behaviour of such a blend with a continuous interfacial coverage can be compared to that of high-impact polystyrene (HIPS). In HIPS, the PB particles inside the PS matrix again show sub-inclusions of PS. Nevertheless, this more complex dispersed phase can be treated as a single PB particle, i.e. the modulus of the PS sub-inclusions has no effect on the elastic behaviour of the overall blend [47]. In the case of the compatibilised PPE/SAN, this particular morphology can be described as follows:

$$E_{PPE/SAN/SBM} = \phi_{SAN}E_{SAN} + \phi_{PMMA}E_{PMMA} + (\phi_{PPE} + \phi_{PS} + \phi_{PB})E_{PB}. \quad (9)$$

This theoretical prediction leads to a significantly lower blend modulus, as shown in Fig. 7a. The experimental modulus of the PPE/SAN 60/40 blend compatibilised with 20 wt% of SBM2 does indeed fall between the different predictions, accurately reflecting the structural features at the interface. A similar trend can be seen for blends compatibilised with SBM1 and SBM4 (Fig. 6b), again in good agreement with their morphological characteristics [19].

In contrast, the experimental modulus values of the PPE/SAN blends compatibilised with SBM3 remain close to the theoretical predictions based on a discontinuous interfacial coverage, as shown in Fig. 7b. Yet, this particular system showed micellation in the PPE phase, an effect that induces a small reduction in blend modulus due to the inclusions of PB-covered PMMA [19,47]. This morphological situation can be considered by a similar approach as in Eq. 8:

$$E_{PPE/SAN/SBM} = \phi_{PPE}E_{PPE} + \phi_{SAN}E_{SAN} + \phi_{PS}E_{PS} + (\phi_{PB} + \phi_{PMMA})E_{PB}. \qquad (10)$$

Again, the strong specific interactions between PPE and PS can be taken into account:

$$E_{PPE/SAN/SBM} = \phi_{PPE}E_{PPE} + \beta_{PPE/PS}\phi_{PPE}\phi_{PS} + \phi_{PS}E_{PS} + \phi_{SAN}E_{SAN} + (\phi_{PB} + \phi_{PMMA})E_{PB}. \qquad (11)$$

The experimental data at high SBM3 contents appear to accurately reflect the blend morphology, indicated by a good agreement with the theoretical predictions including the micellation effects and the PPE/PS interactions.

3.2.3 Inelastic properties of PPE/SAN blends (high-strain behaviour)

In addition to the discussed low-strain behaviour of the PPE/SAN/SBM blends, the performance at elevated strain levels shows interesting correlations with the blend morphologies. As verified by the representative stress-strain curves for the PPE/SAN blends compatibilised with 20 wt% of the different SBM (Fig. 8a) and by the corresponding data summarised in Table 4, almost all compatibilised blends show a ductile tensile behaviour. Consequently, the yield stress of these materials corresponds to the tensile strength. The only exception is the PPE/SAN blend containing 5 wt% of SBM4 showing a brittle behaviour.

In most cases, the elongation at break of the PPE/SAN 60/40 blend system increases with the addition of the SBM triblock terpolymers (Table 4). Simultaneously, the scattering is generally reduced, indicating a higher stability of the morphology during injection-moulding [19]. For blends of PPE/SAN and SBM1, the elongation at break is significantly enhanced at 5 wt% of SBM1 already and remains at an even higher and rather constant level for 10 and 20 wt%. Similarly, the addition of SBM2 also leads to an identical increase for 5 wt% of the triblock terpolymer, while a slight reduction of elongation at break is observed at elevated SBM2 contents. In the case of compatibilisation by SBM3, the elongation at break is similar to the uncompatibilised blend for low SBM contents, whereas higher values are observed for elevated SBM3 contents. It is reasonable to relate this particular behaviour to the continuity of the PPE phase which is continuously increased by the addition of SBM3. Finally, the addition of

SBM4 initially embrittles the blend; whereas SBM contents approaching 20 wt% lead to significant enhancements of the elongation at break. It is interesting to note that the compatibilisation by 20 wt% of SBM leads to similar values for SBM2 and SBM4, while higher values are observed for systems showing micelles either in the PPE (SBM3) or the SAN (SBM1). A more explicit, micromechanical explanation of the materials properties and a correlation to the blend morphology is given in section 3.2.4.

Compared to the elastic behaviour, the theoretical prediction of the yield stress of such complex blend systems is even more challenging. In a first attempt to establish boundaries for the materials behaviour, some factors such as the influence of the end blocks on the respective blend phases are neglected. In the simplest case, neglecting the small contribution of the PB block and assuming optimum compatibilisation, the yield stress of the blend, $\sigma_{PPE/SAN/SBM}$, can be predicted using the parallel model:

$$\sigma_{PPE/SAN/SBM} = \sigma_{b,SAN}\left(\phi_{SAN} + \phi_{PMMA}\right) + \sigma_{y,PPE}\left(\phi_{PPE} + \phi_{PS}\right). \qquad (12)$$

The more sophisticated Ishai-Cohen model [48] is often used to predict the yield stress of a single-phase material containing spherical, low-modulus inclusions such as PB with no phase adhesion to the matrix. Applying this model to the PPE/SAN/SBM blends and considering the discontinuous contribution of the PB at the interface (raspberry morphology), it is reasonable to assume that PB equally contributes to the reduction of the yield strength of both the PPE and SAN phase. Considering a parallel model, the yield stress can then be expressed as follows:

$$\sigma_{PPE/SAN/SBM} = \sigma_{b,SAN}\left(1-1.21\left(\frac{\phi_{PB}}{2}\right)^{2/3}\right)\left(\phi_{SAN} + \phi_{PMMA}\right) + \sigma_{y,PPE}\left(1-1.21\left(\frac{\phi_{PB}}{2}\right)^{2/3}\right)\left(\phi_{PPE} + \phi_{PS}\right). \qquad (13a)$$

In the case of SBM micellation in the PPE phase, e.g. for SBM3, Eq. 13a has to be modified:

$$\sigma_{PPE/SAN/SBM} = \sigma_{b,SAN}\phi_{SAN} + \sigma_{y,PPE}\left(1-1.21\left(\phi_{PB} + \phi_{PMMA}\right)^{2/3}\right)\left(\phi_{PPE} + \phi_{PS} + \phi_{PB} + \phi_{PMMA}\right). \qquad (13b)$$

And, finally, assuming a dispersed PPE phase with complete interfacial coverage and no phase adhesion of a PB layer, the yield stress can be expressed as:

$$\sigma_{PPE/SAN/SBM} = \sigma_{b,SAN}\left(1-1.21\left(\phi_{PB} + \phi_{PPE} + \phi_{PS}\right)^{2/3}\right). \qquad (13c)$$

It should be noted that, when phase adhesion is present, the value '1.21' in Eqs. 13 is reduced; thus a minor reduction of the yield stress would be predicted in this case.

Both the parallel model (Eq. 12) and the Ishai-Cohen model (Eq. 13a, 13b and 13c) are compared to the experimental values in Fig. 8b. In the case of compatibilisation by SBM3, the yield strength is significantly higher than predicted by Eq. 13b, almost approaching the parallel model (Eq. 12). Such behaviour promotes the presence of significant adhesion between the SBM micelles in the PPE phase and PPE. Presuming a similarly high adhesion for blends compatibilised by the other SBM grades, the yield strength should be between the boundaries of Eq. 12 and Eq. 13a. Indeed, the experimental values excellently satisfy this assumption. Moreover, the dependence of the yield strength on the SBM content, in particular the higher reduction at elevated weight fraction, is supposed to be a result of the altered microstructure of the blend, e.g. the increasing continuity of the PB layer, as previously described for the modulus behaviour. Further investigations are desirable to even more precisely describe the yield stress behaviour of PPE/SAN/SBM blends; nevertheless, these initial approaches taken here to model the materials properties provide first valuable explanations and insights.

3.2.4 Deformation mechanism of compatibilised PPE/SAN/SBM blends (micromechanics)

In order to discuss the fracture phenomena of the compatibilised PPE/SAN blends as a function of the type and content of the SBM triblock terpolymers in detail, four main factors need to be considered: the blend microstructure (continuity of the phases, anisotropy, phase sizes, molecular orientation of each phase) [32,34-38], the interfacial situation ("raspberry morphology") [3-7,18,19], the influence of the SBM on the properties of the blend constituents PPE and SAN [49,50] and, strongly linked to the previous issues, the role of SBM as a toughening agent. Such a magnitude of variables is typically encountered in the compatibilisation of polymer blends by block copolymers, as compositional variations of the compatibiliser strongly affect the fracture behaviour of the overall blend due to the altered micro- and nanostructures [51]. Although the picture is further complicated by the interdependence of these factors, the following discussion is aimed at establishing some general correlations between the compatibilisation efficiency of the various SBM types and the resulting overall blend performance as presented so far.

As discussed in section 3.1, the ductility of neat PPE/SAN blends can be improved both by reduced phase sizes as well as an increased continuity of the PPE phase. However, the anisotropy of the blend morphology also influences the mechanical properties [30] as highly-oriented ductile phases often lead to a more ductile performance. As demonstrated, the addition of the various SBM grades does indeed alter the microstructure of the PPE/SAN blend

[19]. Yet, both the reduction in average phase size as well as in the degree of orientation and continuity depend on the SBM composition and content.

In addition, the interfacial properties between the two components also have a strong impact on the load-transfer capability. In case of an interfacial enrichment by SBM triblock terpolymers, previous studies of Brown et al. [18] already demonstrated a pronounced reduction of the interfacial toughness at a low layer thickness, whereas slight improvements in toughness were observed at an elevated interfacial thickness (exceeding 40 nm for the particular PPE/SAN system). In contrast, selective micellation of the triblock terpolymer in the PPE phase degrades the interfacial properties of PPE/SAN blends as the interface is then formed between the binary PPE/PS and the SAN phase, respectively [21].

Micelle formation of the SBM in either the PPE or the SAN phase also significantly alters the intrinsic toughness of these two phases. The triblock terpolymer consequently acts similar to well-established toughening agents by improving the ductility of the respective blend component [42,52,53]. Additionally, the critical ligament thickness is increased and, thus, plastic deformation even at elevated phase sizes is ensured [42].

Lastly, the particular “raspberry morphology” at the interface influences the deformation behaviour, although the deformation mechanism is not fully understood yet. Investigating a similar system, Flaris et al. [54] proposed two deformation mechanisms for polypropylene/polyethylene (PP/PE) blends compatibilised by ethylene-propylene copolymers (EP) forming an interfacial layer: (1) craze and deformation initiation in the matrix due to soft particles, and (2) drawing of the PE inclusions. It appears reasonable to anticipate similar phenomena to occur in the present PPE/SAN/SBM systems. The elastomeric PB layer at the interface can initiate deformation in the continuous phase due to localised stress concentrations (even in both phases in the case of co-continuous morphologies) [1,48,52,53] as well as induce drawing of the ductile PPE phase.

All of these factors are altered to a different extent depending on SBM type and content. In the case of triblock terpolymers such as SBM1, SBM2 and SBM4 with similar end block lengths, the high compatibilisation efficiency ensures a pronounced localisation of the SBM at the interface as well as a significant reduction of both the blend phase size and anisotropy. Moreover, the continuity of the PPE phase is further increased as compared to the uncompatibilised PPE/SAN blend. Yet, some micelle formation also occurs [19]. All these microstructural features promote the observed plastic deformation behaviour of the PPE/SAN blend. However, the mechanical tensile data of those PPE/SAN blends compatibilised with low con-

tents of SBM4 indicate that a sufficient length of the middle PB block is necessary in order to ensure a sufficient interfacial thickness, in agreement with the results by Brown et al. [18].

The blends compatibilised by SBM3 show a remarkably different behaviour. In addition to a generally coarser blend morphology, the triblock terpolymer induces a pronounced micelle formation in the PPE phase which, in turn, leads to an interface formed by a binary PPE/PS phase and the SAN. These factors reduce the toughness of the system but, on the other hand, the significantly increased continuity of the PPE phase and even co-continuous blend characteristics at elevated SBM contents explain the observed ductile blend behaviour [32,34-37]. As such, the latter factors dominate the deformation behaviour and lead to the pronounced plasticity as well as high elongations at break.

3.2.5 Modulus vs. fracture energy of PPE/SAN/SBM blends

A suitable combination of both a high stiffness and toughness of a material is of key importance for a given application. An overview plot of tensile modulus vs. fracture energy of all blend systems as obtained from the static tensile tests at room temperature is presented in Fig. 9. As discussed before, the stiffness of all materials decreases with increasing SBM content, independent of the triblock terpolymer used for the compatibilisation. The toughness of blends compatibilised by SBM1 and SBM2, however, is nearly independent of SBM content, but is significantly higher than that of the neat PPE/SAN 60/40 blend. In contrast, the toughness of blends compatibilised by SBM3 and SBM4 continuously increases by the addition of these triblock terpolymers although blend systems containing 5 wt% of SBM3 as well as 5 and 10 wt% of SBM4 show fracture energies below that of the uncompatibilised blend. The same trend is observed for the strain at break due to the direct relationship between these two properties.

Thus, one could argue that materials compatibilised by SBM3 are a good choice for a given application, as these blend systems combine both a high modulus and an enhanced ductility. Nevertheless, as yet, this conclusion only holds for injection-moulded specimens where a tensile load is applied in the flow direction. In order to further elucidate the aforementioned superposition of orientation effects and morphological aspects, detailed investigations of the deformation behaviour parallel and perpendicular to the injection-direction are required. Fatigue crack propagation (FCP) experiments are a sophisticated and well-suited characterisation method to analyse such toughness issues in multiple directions.

3.3 Fatigue crack propagation (FCP) behaviour and anisotropy of PPE/SAN blends

The concept of fracture mechanics is widely applicable to the analysis of the FCP behaviour in polymer blends, as the majority of these materials are capable of sustaining a large amount of sub-critical crack growth prior to fracture. This particular characterisation method not only provides further insights into the deformation mechanisms of the investigated blend materials [1,54,55], but also helps to describe the anisotropic mechanical blend behaviour. In addition to studies on injection-moulded tensile specimens, the influence of orientation effects can thus be more accurately taken into account [54,55].

The FCP behaviour is generally described by a double-logarithmic plot of the fatigue crack growth rate $\frac{da}{dN}$ as a function of the amplitude of the stress intensity factor ΔK acting at the crack tip [23], where the parameter a denotes the crack length. The characteristic plots emphasise three discrete regimes: (1) the threshold regime indicating the initiation of the crack growth K_{th}, (2) the regime of stable crack growth, and (3) the fast fracture regime associated with the critical stress intensity K_{Ic}. The regime of stable crack growth is also referred to as the Paris regime and shows a power-law behaviour described by the relationship [23]:

$$\frac{da}{dN} = C\,\Delta K^{n} \qquad (14)$$

where C and n represent the crack growth rate at $\Delta K = 1$ MPa $m^{1/2}$ and the slope of the curve on the double-logarithmic scale, respectively.

The values observed for the neat PPE and SAN materials are summarised in Tab. 5. As can be seen, PPE shows both an improved threshold behaviour (K_{th}) and a higher critical stress intensity (K_{Ic}) as compared to the more brittle SAN. The critical stress intensity of SAN (1.96 MPa $m^{1/2}$) observed here for an acrylonitrile content of 19 wt% is in reasonable agreement with data shown by Kim et al. [56]. More precisely, Kim at al. reported a linear relationship between the critical stress intensity and the acrylonitrile content, revealing an interpolated value of 1.94 MPa $m^{1/2}$ for an acrylonitrile content of 19 wt%. The minor deviation can be regarded to be within experimental scattering. Further interesting features can be seen for the uncompatibilised PPE/SAN 60/40 blend. For a crack propagation both parallel as well as perpendicular to the injection-direction, the threshold regime of the blend is similar to that observed for the neat SAN; however, the stable crack growth region indicates a significantly faster crack growth parallel to the injection-direction [54,55]. Furthermore, the critical stress intensity of this particular blend in the parallel direction is even lower than that of either neat

PPE or SAN. In contrast, the performance of both base materials is exceeded when crack growth in the blend occurs perpendicular to the injection-direction.

In order to provide a deeper insight into the FCP behaviour of the blend, the respective curves of the PPE/SAN blends are shown in Fig. 10. Besides the test results discussed above, the blend investigated normal to the injection-direction reveals a pronounced scattering in the data, in particular at elevated stress intensities. This behaviour is typically associated with crack deflection and bridging effects of the more ductile phase and was verified by electron microscopic observations of the fracture surfaces of the specimens after testing.

In order to properly analyse the influence of orientation effects, SEM micrographs of the core region were taken for both FCP directions at a constant crack growth rate of 10^{-4} mm/cycle (Fig. 11). In case of crack propagation parallel to the injection-direction (Fig. 11a), SAN appears as the continuous (brighter) phase surrounding the complex, rather disperse PPE phase with a notable degree of continuity. Distinct interfacial debonding between the two blend components can be detected. As the SAN features a small extent of plastic deformation, the crack appears to have propagated through the PPE phase. Closer inspection of the PPE phase reveals the previously described sub-inclusions of SAN which show a pronounced shear deformation; a behaviour that can be correlated with the cold-drawing concept.

Crack propagation perpendicular to the injection-direction leads to a strongly altered micromechanical response of the blend (Fig. 11b). A significantly reduced interfacial failure can be detected, and both PPE and SAN show pronounced plastic deformation. In particular, PPE appears as the highly elongated blend phase, capable to further increase the resistance against crack propagation by bridging and deflection mechanisms [1].

Summarising the FCP behaviour of the PPE/SAN 60/40 blends, the deformation phenomena can be correlated with the concepts outlined in chapter 3.1.3. The phase adhesion between PPE and SAN appears sufficiently high to allow load transfer between the two phases, as long as the more ductile PPE phase shows continuous characteristics perpendicular to the crack growth direction. The materials response can thus be explained by the cold-drawing concept and by phenomena such as bridging mechanisms similarly encountered in layer- and fibre-like blend morphologies. As a result, both phases can undergo plastic deformation leading to a mechanical performance surpassing the properties of the neat polymers. These concepts do not hold in the case of crack growth parallel to the injection-direction; here, the lower degree of continuity prevents the described phenomena and leads to poor mechanical properties. Injection-moulded PPE/SAN blends must thus be classified as strongly anisotropic materials.

3.4 Effect of compatibilisation on the fatigue crack growth behaviour

The comparison of different crack propagation directions revealed that the base blend material is most sensitive to cracks propagating parallel to the injection-direction. Further investigations of the compatibilised PPE/SAN blends were therefore focussed on this weakest link. As the impact of compatibilisation on the fracture mechanical behaviour can be assumed to be most pronounced at the highest SBM content of 20 wt%, the respective properties of these blends were analysed and are summarised in Table 6.

While the threshold regime is shifted to higher stress intensities for all blends, a notable improvement is only observed for blends containing SBM2 and SBM4; those systems previously identified to show the best compatibilisation efficiency. Similar results can be seen for the amplitude of the critical stress intensity factor, as the compatibilisation by SBM1, SBM4 and, in particular, by SBM2 leads to a pronounced increase in K_{Ic} as compared to the uncompatibilised blend (+ 38%). Furthermore, the crack growth rate at 1 MPa $m^{1/2}$ is significantly reduced, in the case of SBM1 and SBM4 by more than 50%, and for blends based on SBM2 even by 80%. In contrast, a similar improvement is not observed for blends compatibilised by SBM3. Here, the severe reduction of the critical stress intensity as well as the strong increase in the crack propagation rate (as indicated by the parameter C) reveal significantly worse properties of the modified blend as compared to the base PPE/SAN 60/40 blend.

In this context, a comparison of the FCP curves of PPE/SAN blends compatibilised by SBM2 and SBM3 highlight the upper and lower bounds of the mechanical performance (Fig. 12). SBM2 serves as a highly suitable compatibilising agent located at the interface between PPE and SAN, whereas SBM3 tends to form micelles in PPE [19]. As already discussed, this behaviour strongly affects the FCP behaviour. In order to correlate the observed mechanical behaviour to the respective deformation mechanisms of the compatibilised PPE/SAN blends, a more detailed analysis of the fracture surfaces is required.

SEM micrographs of the core region of both materials were taken at a constant crack growth rate of 10^{-4} mm/cycle (Fig. 13). However, due to the reduced phase size following the compatibilisation step, differentiation of the respective blend phases by SEM is complicated. The PPE/SAN/SBM2 blend (Fig. 13a) reveals a rather ductile behaviour of the finely structured morphology. Both PPE and SAN undergo substantial cooperative plastic deformation and, in particular, no evidence for an interfacial failure or anisotropy of the blend can be observed. In contrast, the SEM micrographs showing PPE/SAN blends compatibilised by SBM3 (Fig. 13b) indicate distinct interfacial debonding and strongly deformed domains alternating with non-

deformed regions. This behaviour results in a rather rough fracture surface. Furthermore, an anisotropic morphology can be detected which is similar to that of the uncompatibilised blend.

The effects determining the FCP performance can again be attributed to the blend morphology, more precisely, to the compatibilisation efficiency of the triblock terpolymers and to the isotropy of the specimen; factors that strongly influence the deformation mechanism as discussed in section 3.2. In the case of SBM3, which mostly forms micelles in PPE, the interfacial adhesion between the two blend phases is decreased as a result of the PS enrichment in PPE [21]. The low load transfer between PPE and SAN thus enhances interfacial failure. As the crack proceeds parallel to the highly-oriented PPE domains, this effect becomes – in contrast to the discussed tensile properties – highly detrimental to the mechanical performance.

The FCP behaviour of the well-compatibilised blends strongly differs with regard to the deformation mechanism. At these elevated SBM contents of 20 wt%, the interfacial width is assumed to be sufficiently high to increase rather than decrease the interfacial strength [18]. The triblock terpolymers not only significantly reduce the phase size as well as the anisotropy, but can also initiate local plastic deformation of the blend; a phenomenon similar to that observed in well-known polymeric systems toughened by core-shell impact modifiers such as HIPS or ABS. In combination, the ductile behaviour of the blend can be notably enhanced, leading to a superior performance as compared to the uncompatibilised blend both perpendicular as well as parallel to the injection-direction. A further evaluation of the FCP behaviour of the compatibilised blends however, e.g. in order to analyse the influence of the SBM content and the deformation characteristics of the skin layers, is beyond the scope of the present paper.

4 CONCLUSIONS

The mechanical property profile of immiscible PPE/SAN blends as well as the influence of subsequent compatibilisation using tailored SBM triblock terpolymers on both the static tensile properties as well as on the fatigue crack propagation behaviour of these blends were evaluated in detail. In line with the potential commercial interest in these particular systems, all polymer blends were prepared by melt-compounding using twin-screw extrusion and subsequent injection-moulding.

Immiscible PPE/SAN blends revealed brittle characteristics for SAN-rich compositions, while a brittle-to-ductile transition was detected for increasing PPE contents up to 60 wt%, ap-

proaching co-continuity of the system. The ductile behaviour, as indicated by a reasonably high ultimate tensile strain, can be related both to the particular blend morphology as well as to the intrinsic properties of the constituents. The micromechanical deformation mechanism of such ductile blends can be elucidated by the cold-drawing concept. Similarly, the ultimate strength as well as the modulus behaviour are in good agreement with micromechanical models, showing a rather linear dependence on blend composition. PPE/SAN 60/40 blends were selected as a most promising system for the compatibilisation by SBM triblock terpolymers.

The compatibilisation step generally further enhanced the ductility of the blends, as indicated by an increase in ultimate strain and fracture energy. However, a comparative evaluation of the performance of the various tailored SBM triblock terpolymers revealed that the improved toughness originates from different morphological features influencing the micromechanical behaviour. In case of block copolymers with nearly symmetric end blocks (SBM1, SBM2, SBM4), the high compatibilisation effectiveness leads to an interfacial enrichment and a reduced phase size; factors that beneficially contribute to the toughness. In contrast, triblock terpolymers with a significantly higher PS content (SBM3) lead to micelle formation in the PPE. This micellation results in an improved toughness and a higher continuity of the PPE phase, also advantageous for the ultimate performance of the overall blend. In addition, the modulus and strength remained at a remarkably high level as compared to the blends compatibilised by SBM1 and SBM2. However, the corresponding specimens revealed a pronounced anisotropy, similar to the uncompatibilised blend.

In order to sensitively evaluate such orientation effects, fatigue crack propagation experiments parallel to the direction of injection moulding, the weakest link in the blend, were performed. In contrast to the static tensile behaviour, the FCP analysis highlighted further distinct differences between the SBM grades. Only SBM triblock terpolymers with symmetric end blocks and sufficiently high PB contents (SBM2) were able to significantly improve the resistance against crack propagation, whereas SBM materials with a longer PS block (SBM3) strongly degraded the materials performance. Symmetric SBM triblock terpolymers can thus be regarded as compatibilisers providing a superior performance balance between strength, modulus, toughness and isotropy. In particular, compatibilisation by SBM2 indicates an improved toughness of PPE/SAN blends, as comparatively summarised in Fig. 14.

The systematic correlation of the blend morphology with the resulting mechanical properties presented in this study has allowed an identification of suitable SBM compatibilisation agents for immiscible PPE/SAN blends, providing an improved toughness as well as fatigue crack

growth resistance while maintaining a high strength as well as modulus. As such, the fundamental relationships between microstructure and deformation mechanisms demonstrated here for such compatibilised PPE/SAN systems are not only valid for this particular system but contribute to the understanding of the micromechanical performance of complex blend systems in general. Further beneficial features of such well-compatibilised and nanostructured PPE/SAN blends are currently exploited for the development of cellular blend morphologies.

5 ACKNOWLEDGEMENTS

This work has been supported by the German Science Foundation (Deutsche Forschungsgemeinschaft DFG, SFB 481, project A10). The authors are grateful to Dr. M. Weber, BASF AG (Ludwigshafen) and to MEP Europe (Düsseldorf) for providing the SAN and PPE, respectively. Furthermore, the authors are indebted to D. Danz (Macromolecular Chemistry II, University of Bayreuth) for synthesising the SBM triblock terpolymers, to C. Kunert (Polymer Engineering, University of Bayreuth, SFB 481, Z2, respectively) for the TEM investigations, and to F. Fischer (Polymer Engineering, University of Bayreuth) for his experimental support with regard to the fatigue crack growth investigations.

REFERENCES

[1] Paul DR, Bucknall CB. Polymer blends. 2nd ed. New York: John Wiley & Sons, 2000 (volume 1, 2).

[2] Utracki LA. Polymer blends handbook. 1st ed. Kluwer Academic Publishers, 2002 (volume 1, 2).

[3] Auschra C, Stadler R. Macromolecules 1993;26(24):6364-6377.

[4] Gottschalk A, Muhlbach K, Seitz F, Stadler R, Auschra C. Macromolecular Symposia 1994;83:127-146.

[5] Merfeld GD, Karim A, Majumdar B, Satija SK, Paul DR. Journal of Polymer Science Part B-Polymer Physics 1998;36(17):3115-3125.

[6] Lach R, Grellmann W, Weidisch R, Altstadt V, Kirschnick T, Ott H, Stadler R, Mehler C. Journal of Applied Polymer Science 2000;78(11):2037-2045.

[7] Kirschnick T, Gottschalk A, Ott H, Abetz V, Puskas J, Altstädt V. Polymer 2004;45(16):5653-5660.

[8] Fekete E, Foldes E, Damsits F, Pukanszky B. Polymer Bulletin 2000;44(4):363-370.

[9] Lee CH, Lee SG, Kang SW, Yun S, Kim JH, Choe S. Polymer-Korea 1999;23(1):98-104.

[10] Milner ST, Xi HW. Journal of Rheology 1996;40(4):663-687.

[11] Paul DR, Newman S. Polymer blends. 1st ed. New York: Academic Press, 1978 (Volume 2).

[12] Creton C, Kramer EJ, Hadziioannou G. Macromolecules 1991;24(8):1846-1853.

[13] Anastasiadis SH, Gancarz I, Koberstein JT. Macromolecules 1989;22(3):1449-1453.

[14] Sundararaj U, Macosko CW. Macromolecules 1995;28(8):2647-2657.

[15] Noolandi J, Hong KM. Macromolecules 1982;15(2):482-492.

[16] Auschra C, Stadler R, Voigt-Martin IG. Polymer. 1993;34(10):2081-2093.

[17] Auschra C, Stadler R, Voigt-Martin IG. Polymer. 1993;34(10):2094-2110.

[18] Brown HR, Krappe U, Stadler R. Macromolecules 1996;29(20):6582-6588.

[19] Ruckdäschel H, Sandler, JKW, Altstädt V, Rettig C, Schmalz H, Abetz V, Müller AHE. Polymer 2006;47(8):2772-2790.

[20] Suess M, Kressler J, Kammer HW. Polymer 1987;28(6):957-960.

[21] Wool RP. Polymer Interfaces, 1st ed. Munich: Carl Hanser, 1995 (Chapter 7).

[22] Hertzberg RW, Manson JA. Fatigue of Engineering Plastics. New York: Academic Press, 1980.

[23] Ramsteiner F, Armbrust T. Polymer Testing 2001;20(3):321-327.

[24] Creton C, Kramer EJ, Brown HR, Hui CY. Advances in Polymer Science 2002;156:53-136.

[25] Kolarik J, Lednicky F, Locati G, Fambri L. Polymer Engineering and Science 1997;37(1):128-137.

[26] Paul DR, Newman S. Polymer blends. 1st ed. New York: Academic Press, 1978 (Volume 1).

[27] Takayanagi M, Harima H, Iwata Y. Journal of the Society of Materials Science Japan 1963;12:389.

[28] Nielsen LE. Journal of Applied Physics 1970;41(11):4626-4627.

[29] Kerner EH. Proceedings of the Physical Society of London Section B 1956;69(8):808-

813.

[30] Li ZM, Yang W, Yang SY, Huang R, Yang MB. Journal of Materials Science 2004;39(2):413-431.

[31] Quintens D, Groeninckx G, Guest M, Aerts L. Polymer Engineering and Science 1990;30(2):1474-1483.

[32] Quintens D, Groeninckx G, Guest M, Aerts L. Polymer Engineering and Science 1991;31(16):1207-1214.

[33] Chiang WY, Hwung DS. Polymer Engineering and Science 1987;27(9):632-639.

[34] Kurauchi T, Ohta T. Journal of Materials Science 1984;19(5):1699-1709.

[35] Koo KK, Inoue T, Miyasaka K. Polymer Engineering and Science 1985;25(12):741-746.

[36] Keitz JD, Barlow JW, Paul DR. Journal of Applied Polymer Science 1984;29(10):3131-3145.

[37] Li ZM, Xie BH, Yang SY, Huang R, Yang MB. Journal of Materials Science 2004;39(2):433-443.

[38] Angola JC, Fujita Y, Sakai T, Inoue T. Journal of Polymer Science Part B – Polymer Physics 1988;26(4):807-816.

[39] Takahashi K, Ikeda M, Harakawa K, Tanaka K, Sakai T. Journal of Polymer Science Part B – Polymer Physics 1978;16(3):415-415.

[40] Kerns J, Hsieh A, Hiltner A, Baer E. Journal of Applied Polymer Science 2000;77(7):1545-1557.

[41] Vandersanden, MCM, Buijs LGC, Debie FO, Meijer HEH. Polymer 1994;35(13):2783-2792.

[42] Gregory BL, Siegmann A, Im J, Hiltner A, Baer E. Journal of Materials Science 1987;22(2):532-538.

[43] Kleiner LW, Karasz FE, Macknight WJ. Polymer Engineering and Science 1979;19(7):519-524.

[44] Brandrup J, Immergut EH, Grulke EA. Polymer Handbook. 4th ed. New York: John Wiley & Sons, 1999.

[45] Yee AF. Polymer Engineering and Science 1977;17(3):213-219.

[46] Bucknall CB, Cote FFP, Partridge IK. Journal of Materials Science 1986;21(1):301-306.

[47] Bucknall CB, Davies P, Partridge IK. Journal of Materials Science 1986;21(1):307-313.

[48] Tucker PS, Barlow JW, Paul DR. Macromolecules 1988;21(6):1678-1685.

[49] Kim H, Keskkula H, Paul DR. Polymer 1990;31(5):869-876.

[50] Hermes HE, Higgins JS. Polymer Engineering and Science 1998;38(5)847-856.

[51] Bucknall CB. Toughened plastics. 1st ed. London: Applied Science Publishers, 1977.

[52] Wu SH. Polymer 1985;26(12):1885-1863.

[53] Flaris V, Stachurski ZH. Journal of Applied Polymer Science 1992;45(10):1789-1798.

[54] Bureau NM, Di Francesco E, Denault J, Dickson JI. Polymer Engineering and Science 1999;39(6):1119-1129.

[55] Bureau NM, Dickson JI, Denault J. Journal of Materials Science 1998;33(6):1405-1419.

[56] Kim HS, Keskkula H, Paul DR. Polymer 1991;32(13):2372-2376.

Table(s)

TABLES

Triblock terpolymer		M_n [kg/mol]	$M_{n,S}$ [kg/mol]	$M_{n,B}$ [kg/mol]	$M_{n,M}$ [kg/mol]	1,4-B [%]	M_w/M_n
SBM1	$S_{28}B_{36}M_{36}^{105}$	105	29	38	38	90	1.02
SBM2	$S_{33}B_{34}M_{33}^{94}$	94	31	32	31	90	1.02
SBM3	$S_{50}B_{27}M_{23}^{126}$	126	63	34	29	90	1.02
SBM4	$S_{40}B_{20}M_{40}^{90}$	90	36	18	36	89	1.02

Table 1: Composition of the synthesised triblock terpolymers. The indices denote the composition in weight-%, exponents indicate the number-average molecular weight in kg/mol.

Composition	PPE	SAN	SBM
Uncompatibilised blends	20	80	-
	40	60	-
	50	50	-
	60	40	-
Compatibilised blends	57	38	5
	54	36	10
	48	32	20

Table 2: Composition of the uncompatibilised and the compatibilised PPE/SAN blends. Numbers denote the composition in wt%. Furthermore, 0.1 wt% of a stabiliser was added.

Material	E [GPa]	σ_y [MPa]	ε_y [%]	σ_b [MPa]	ε_b [%]	W [kJ/m^2]
SAN	3.80 ± 0.12	-	-	77.9 ± 0.6	2.93 ± 0.06	27 ± 1
PPE/SAN 20/80	3.47 ± 0.10	-	-	69.9 ± 0.3	2.71 ± 0.03	22 ± 0
PPE/SAN 40/60	3.29 ± 0.06	-	-	73.0 ± 0.3	3.54 ± 0.07	32 ± 1
PPE/SAN 50/50	3.22 ± 0.06	-	-	73.4 ± 0.4	4.01 ± 0.17	39 ± 2
PPE/SAN 60/40	3.08 ± 0.15	72.5 ± 0.4	4.77 ± 0.07	47.9 ± 14.4	40.2 ± 24.5	418 ± 252
PPE	2.50 ± 0.09	71.7 ± 1.6	5.95 ± 0.17	52.2 ± 5.8	69.8 ± 39.0	710 ± 443

Table 3: Tensile properties of the base materials PPE and SAN, respectively, and of the uncompatibilised PPE/SAN blends.

Material	E [GPa]	σ_y [MPa]	ε_y [%]	σ_b [MPa]	ε_b [%]	W [kJ/m^2]
PPE/SAN 60/40	3.08 ± 0.15	72.5 ± 0.4	4.77 ± 0.07	47.9 ± 14.4	40.2 ± 24.5	418 ± 252
+ 5 wt% SBM1	3.01 ± 0.09	70.3 ± 0.2	4.74 ± 0.05	52.8 ± 0.7	76.4 ± 14.6	817 ± 156
+ 10 wt% SBM1	2.84 ± 0.07	66.5 ± 0.2	4.62 ± 0.04	52.6 ± 4.0	97.9 ± 3.0	1022 ± 32
+ 20 wt% SBM1	2.57 ± 0.06	60.1 ± 0.2	4.64 ± 0.06	47.3 ± 8.8	96.8 ± 12.7	944 ± 127
+ 5 wt% SBM2	2.97 ± 0.07	72.3 ± 0.6	4.98 ± 0.11	54.7 ± 2.0	81.1 ± 12.1	890 ± 142
+ 10 wt% SBM2	2.89 ± 0.13	67.3 ± 0.9	4.81 ± 0.37	50.2 ± 3.1	50.5 ± 18.5	524 ± 188
+ 20 wt% SBM2	2.48 ± 0.04	58.5 ± 0.5	4.60 ± 0.04	48.4 ± 0.5	66.4 ± 16.6	642 ± 161
+ 5 wt% SBM3	3.04 ± 0.05	71.7 ± 0.1	4.80 ± 0.04	48.2 ± 3.5	33.7 ± 7.6	360 ± 81
+ 10 wt% SBM3	2.93 ± 0.05	70.5 ± 0.1	4.68 ± 0.22	53.4 ± 9.7	65.0 ± 34.2	755 ± 473
+ 20 wt% SBM3	2.83 ± 0.11	66.9 ± 0.2	4.67 ± 0.08	50.8 ± 3.1	81.8 ± 13.2	843 ± 136
+ 5 wt% SBM4	3.08 ± 0.10	72.0 ± 0.8	4.17 ± 0.54	70.2 ± 4.3	4.2 ± 0.5	49 ± 8
+ 10 wt% SBM4	3.04 ± 0.03	71.2 ± 0.4	4.66 ± 0.08	62.7 ± 12.8	7.3 ± 3.5	81 ± 18
+ 20 wt% SBM4	2.84 ± 0.10	67.4 ± 0.4	4.65 ± 0.08	51.4 ± 1.3	62.2 ± 16.9	652 ± 173

Table 4: Tensile properties of the reference PPE/SAN 60/40 blend and of all compatibilised PPE/SAN/SBM blends.

Material	K_{th} [MPa $m^{1/2}$]	K_{Ic} [MPa $m^{1/2}$]	n [-]	C [10^{-4} mm]
PPE	0.30	2.16	3.1	6.8
SAN (parallel)	0.25	1.96	3.0	3.6
PPE/SAN 60/40 (parallel)	0.24	1.80	3.3	9.2
PPE/SAN 60/40 (perpendicular)	0.22	2.37	2.7	3.9

Table 5: Fatigue crack growth properties of the base materials PPE and SAN, respectively, and of the uncompatibilised PPE/SAN 60/40 blend tested both parallel and perpendicular to the injection-direction. It should be noted that the neat PPE specimen was unoriented due to the preparation by compression-moulding.

Material	K_{th} [MPa $m^{1/2}$]	K_{Ic} [MPa $m^{1/2}$]	n [ ]	C [10^{-4} mm]
PPE/SAN 60/40	0.24	1.80	3.28	9.4
+ 20 wt% SBM1	0.27	1.99	4.35	4.3
+ 20 wt% SBM2	0.32	2.55	3.44	1.7
+ 20 wt% SBM3	0.28	1.07	4.31	17
+ 20 wt% SBM4	0.31	1.92	4.11	4.6

Table 6: Fatigue crack growth properties of the compatibilised PPE/SAN 60/40 blends containing 20 wt% of the various SBM. Data for the uncompatibilised PPE/SAN 60/40 blend are included for comparison. The values reported here correspond to specimens where crack growth was investigated parallel to the injection-direction.

FIGURES

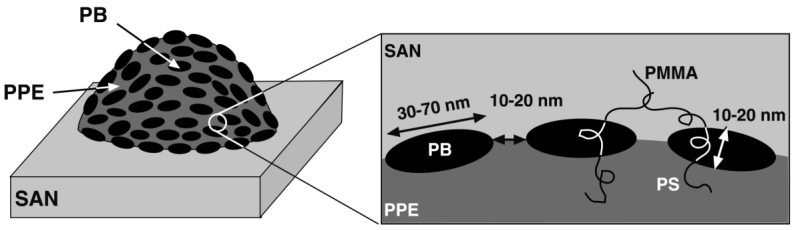

Figure 1: Schematic of the morphological arrangement in PPE/SAN blends compatibilised by SBM triblock terpolymers – "raspberry" morphology.

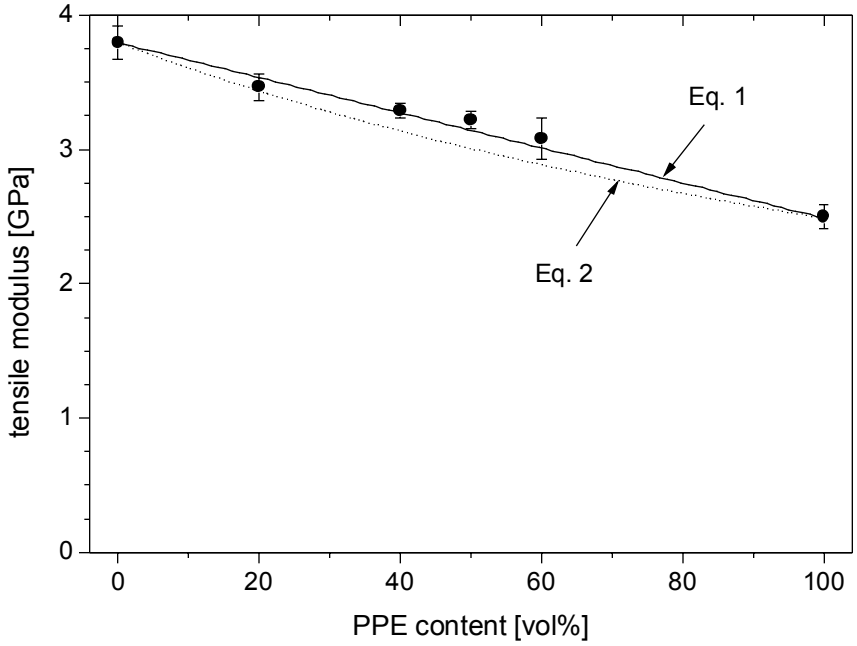

Figure 2: Tensile modulus of PPE/SAN blends as a function of the blend composition. The full and dotted lines correspond to theoretical considerations according to Eqs. 1 and 2, respectively.

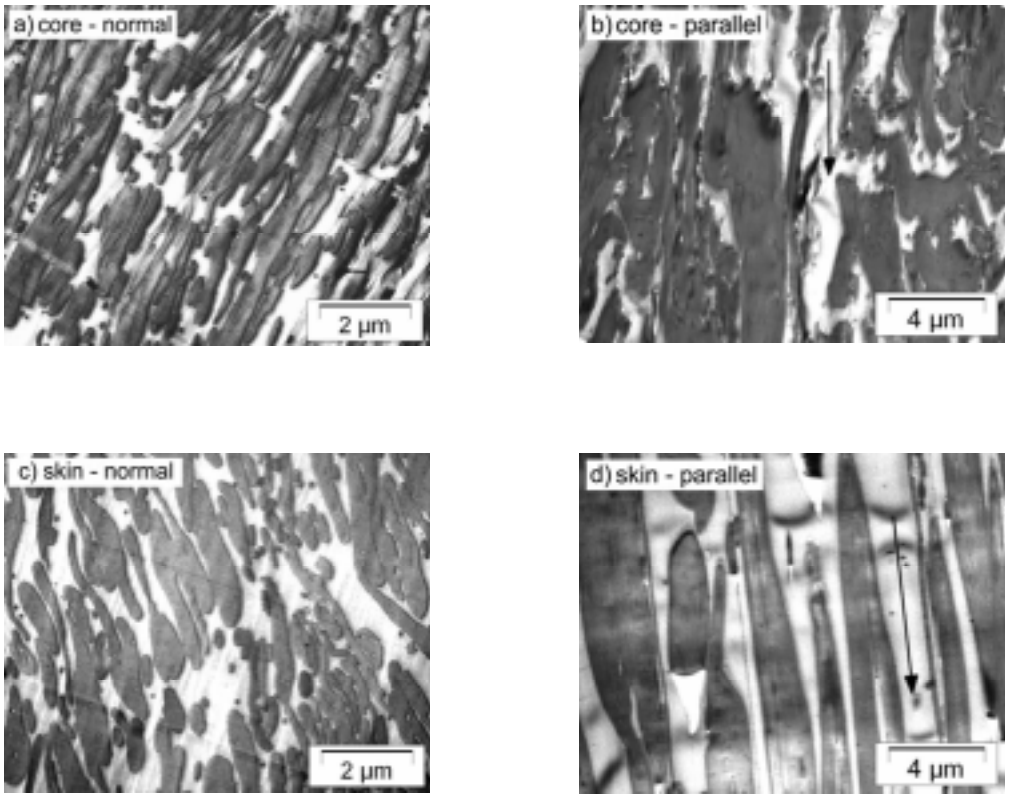

Figure 3: Representative TEM micrographs of the PPE/SAN 60/40 blend following injection-moulding; with the image plane both normal and parallel to the flow direction. Samples were taken at different positions of the parallel section of the tensile bar. The arrows indicate the injection direction. (SAN appears as the bright phase, PPE appears dark).

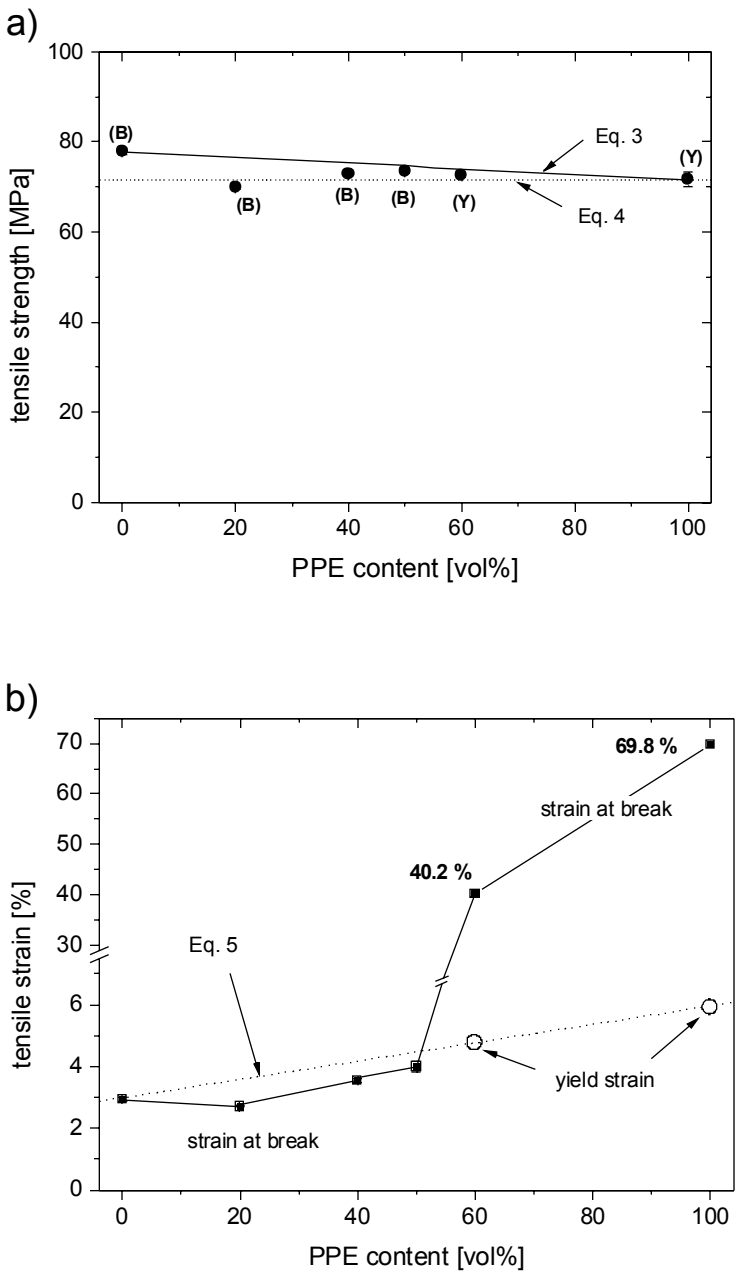

Figure 4: Summary overview of selected tensile properties of the PPE/SAN blends – neat PPE as well as PPE/SAN 60/40 show a tough behaviour (yielding), whereas all other blends are brittle. The abbreviations 'Y' and 'B' denote 'yielding' and 'break' at the shown value, respectively.
(a) Tensile strength of the PPE/SAN blends. The full circles correspond to the experimentally observed values. The lines are calculated according to Eq. 3 (full) and Eq. 4 (dotted).
(b) Strain at break of the PPE/SAN blends (the solid line is drawn to guide the eye). The dotted line is calculated according to Eq. 5. In addition, the yield strain for the PPE/SAN 60/40 blend and for the neat PPE is shown. By reason of clarity, the standard deviation is not shown and can be taken from Table 3.

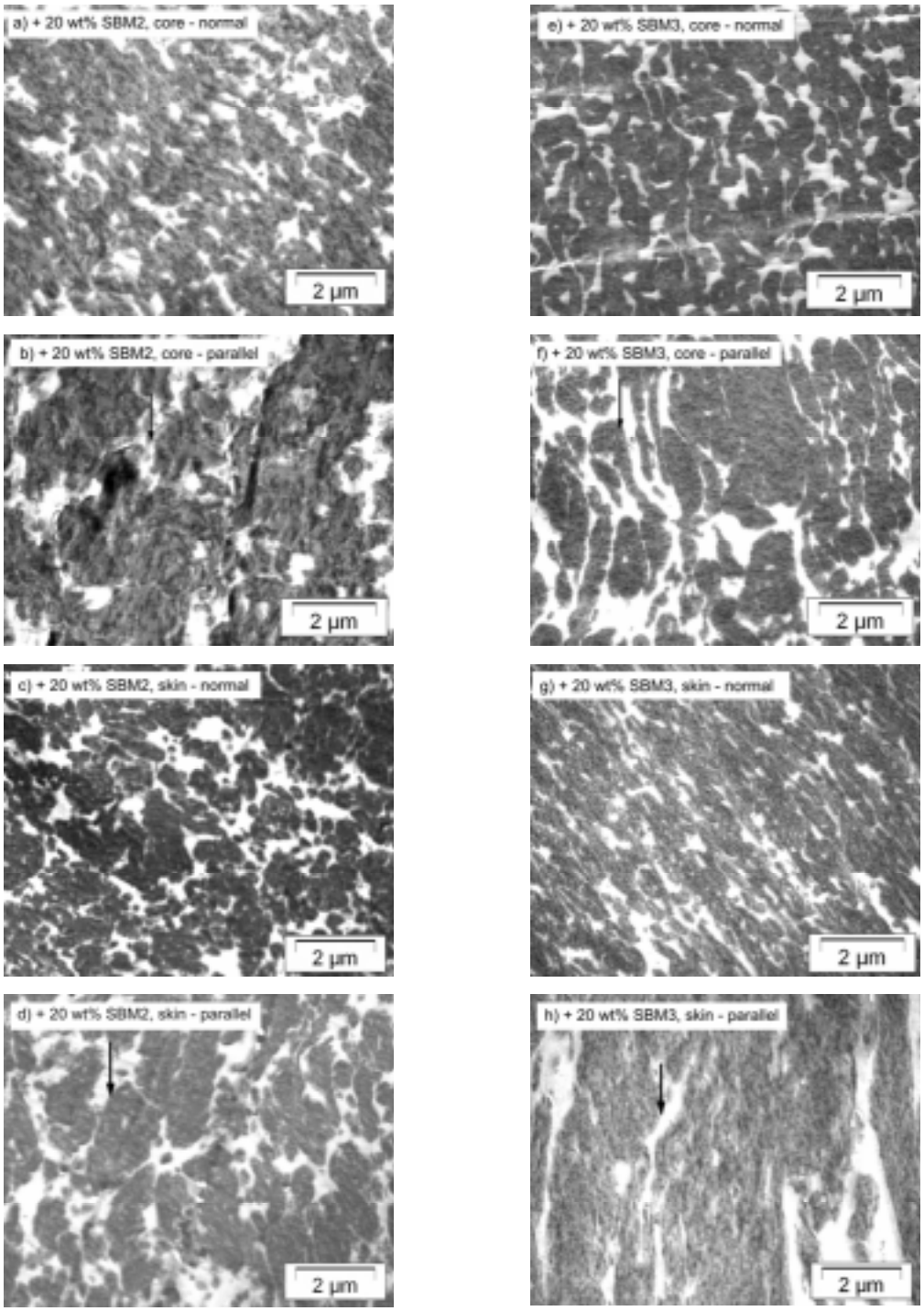

Figure 5: Representative TEM micrographs of compatibilised PPE/SAN 60/40 blends following injection-moulding. Samples were taken at different positions of the parallel section of the tensile bar. (a+e) core region, normal to the flow direction; (b+f) core region, parallel to the flow direction; (c-g) skin region, normal to the flow direction; (d+h) skin region, parallel to the flow direction. (SAN bright, PPE dark).

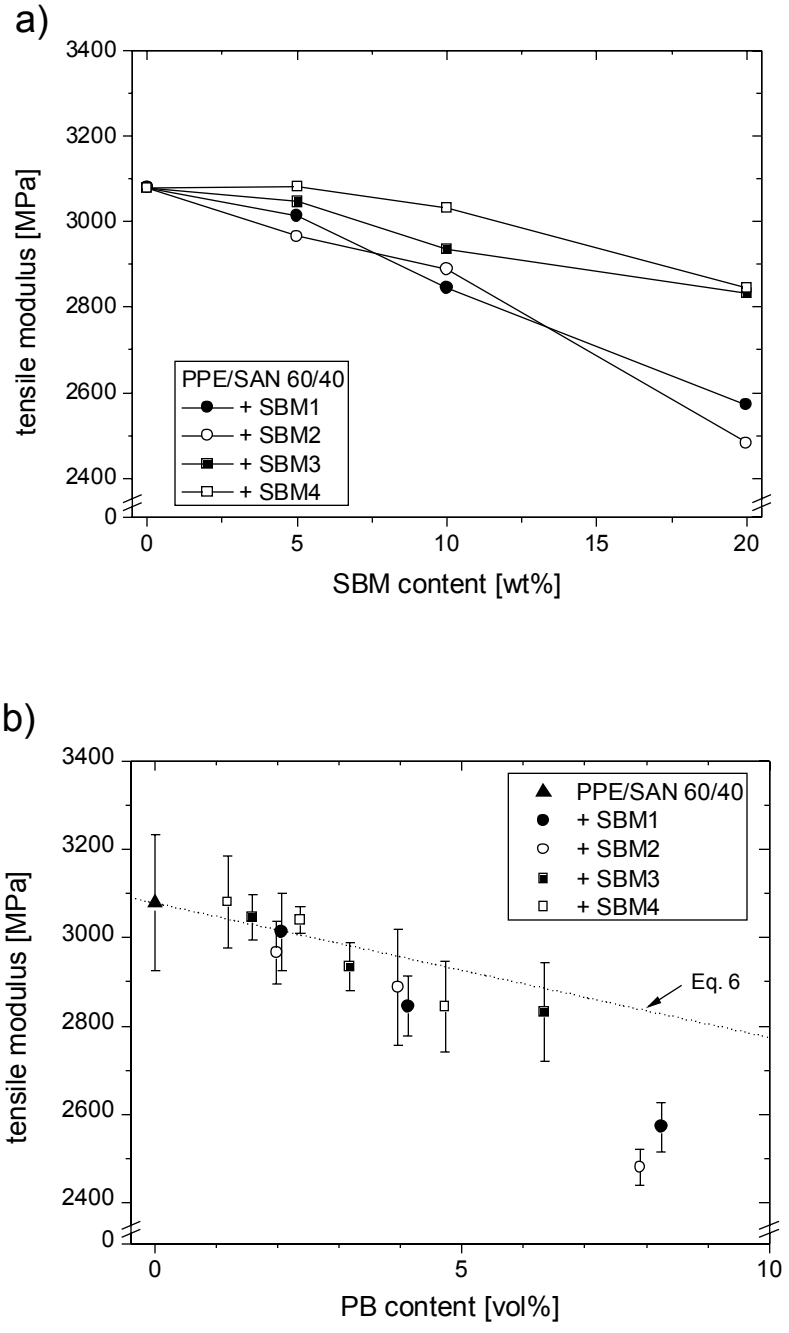

Figure 6: Tensile modulus of compatibilised PPE/SAN blends
(a) as a function of the weight content of SBM.
(b) as a function of the volume content of PB.

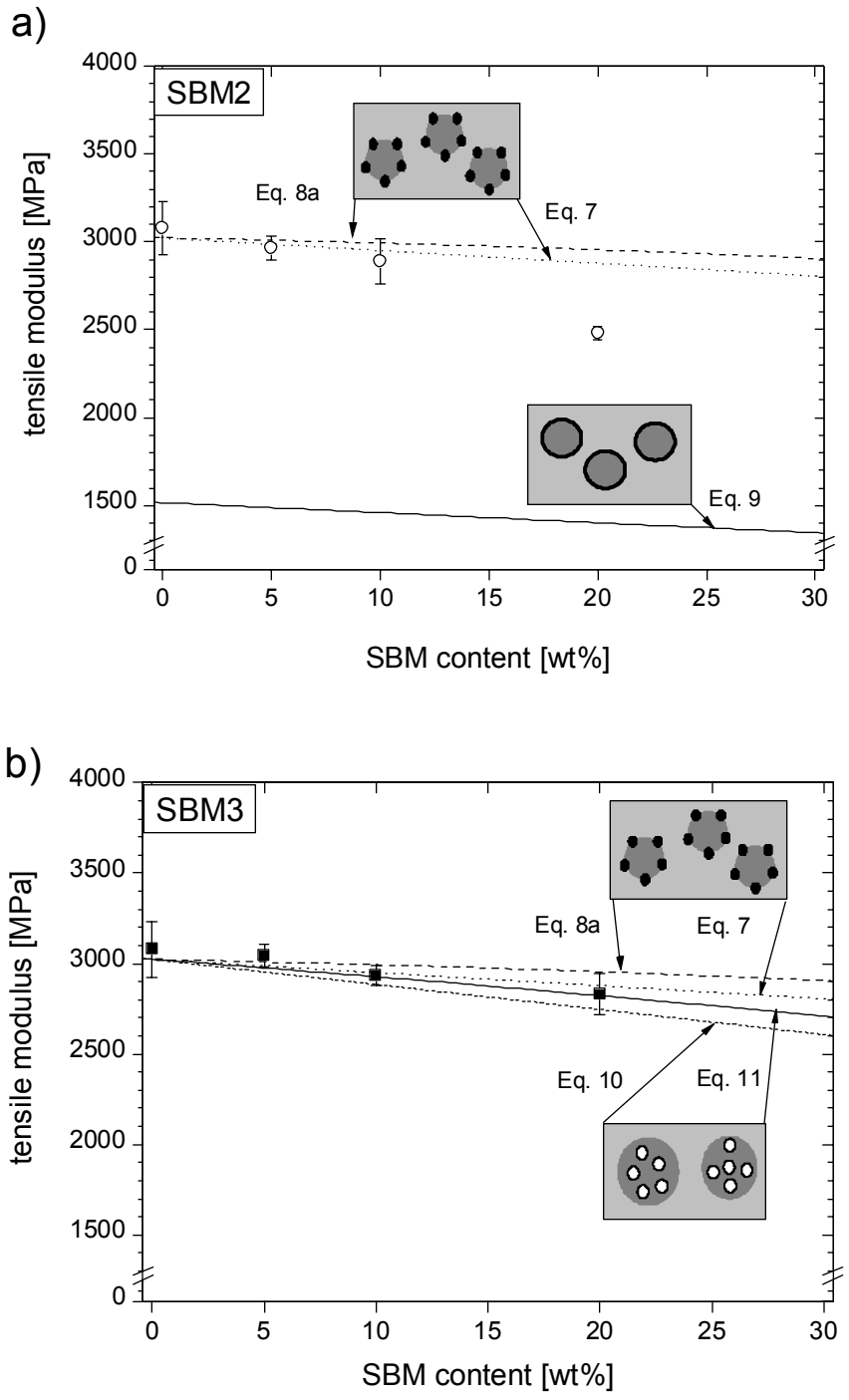

Figure 7: Tensile modulus of compatibilised PPE/SAN blends as a function of the SBM content for SBM2 (a) and SBM3 (b). The various lines correspond to theoretical predictions based on the labelled equations. The schematics represent the corresponding morphological arrangements (dark – PPE phase, bright – SAN phase, black – PB phase; the PMMA appears as white phase in case of micelle formation of SBM in PPE).

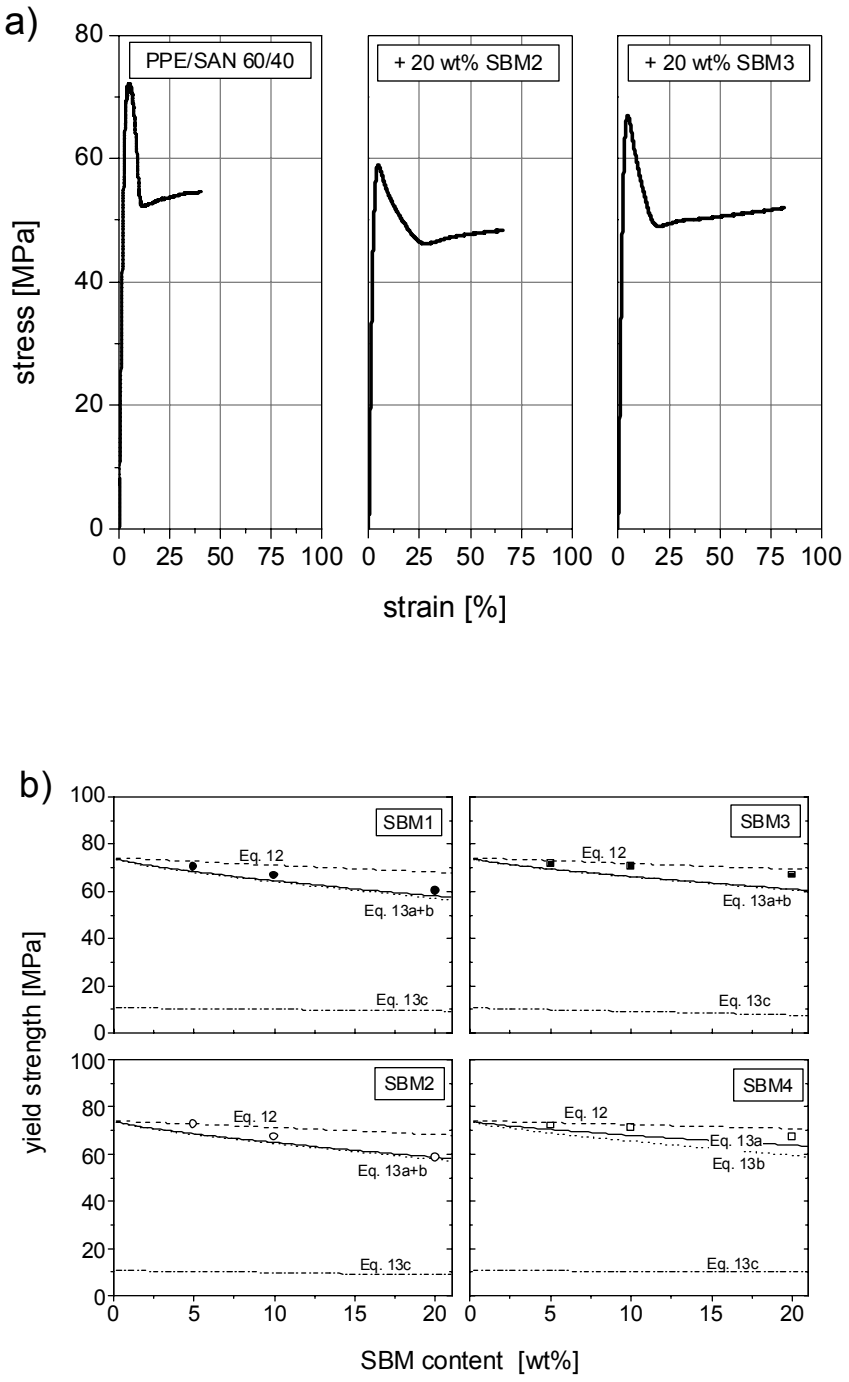

Figure 8: (a) Representative tensile stress-strain curves of the uncompatibilised PPE/SAN 60/40 blend and of blends compatibilised by 20 wt% of SBM2 and SBM3, respectively.
(b) Summary plot of yield strength of compatibilised PPE/SAN blends as a function of the PB volume content. The lines correspond to theoretical predictions based on the respective equations (Eq. 12 – dashed, Eq. 13a – full, Eq. 13b – dotted, Eq. 13c – dashed-dotted).

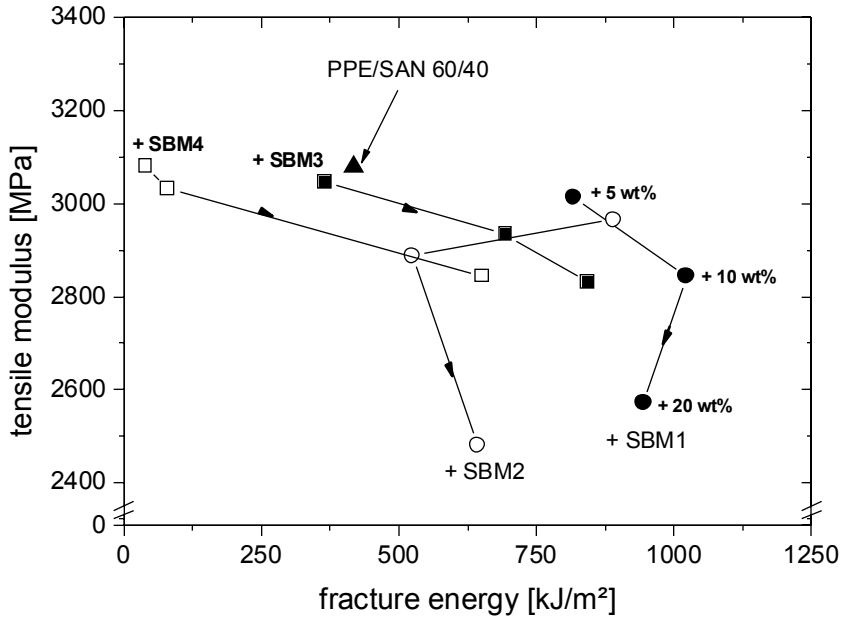

Figure 9: Summary plot of tensile modulus vs. fracture energy for the compatibilised PPE/SAN blends. The arrows indicate an increasing SBM content (5, 10, 20 wt%).

Figure(s)

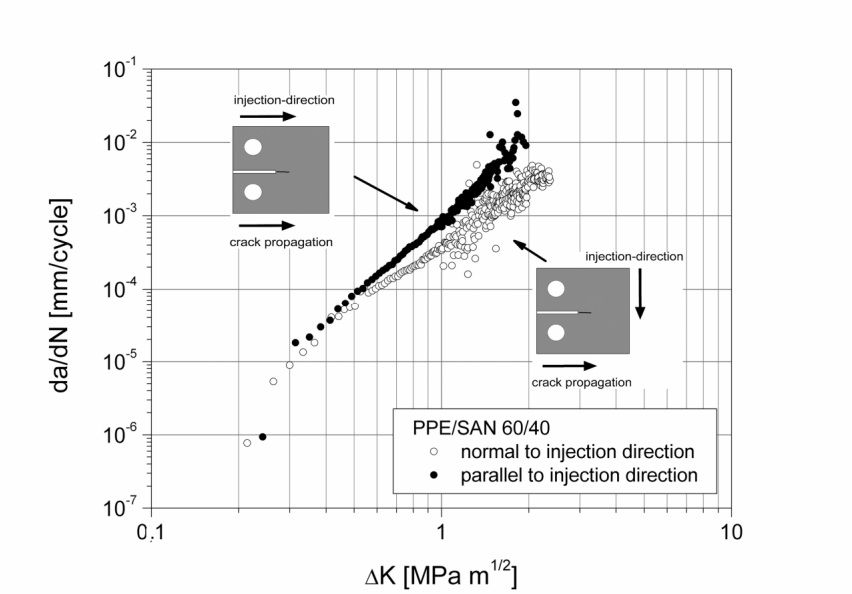

Figure 10: Influence of injection-direction on the fatigue crack growth behaviour of the PPE/SAN 60/40 blend. Full symbols denote crack growth parallel to the injection-direction, open symbols indicate crack growth perpendicular to the injection-direction.

(a) PPE/SAN 60/40 (parallel)

(b) PPE/SAN 60/40 (normal)

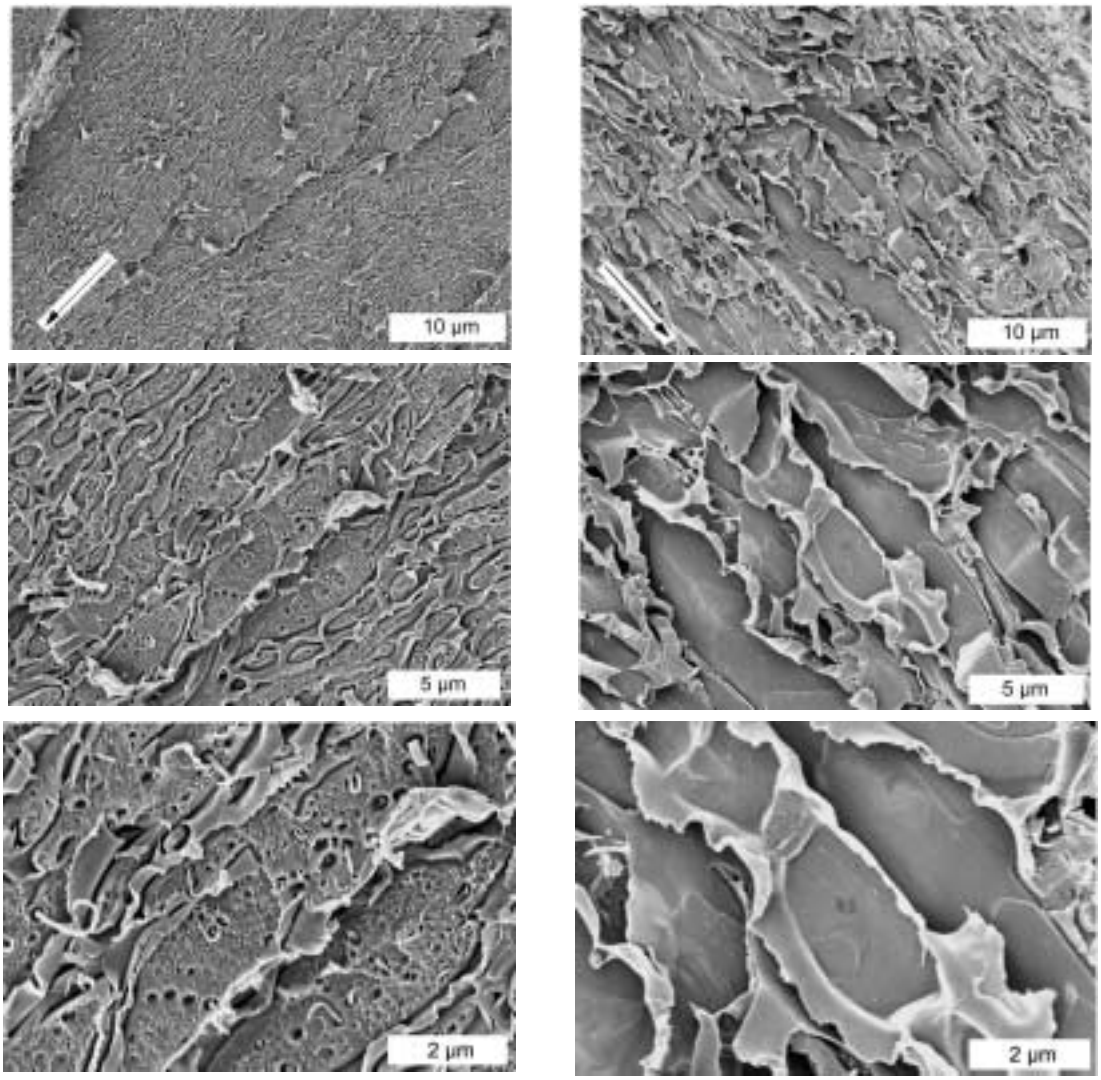

Figure 11: Representative SEM micrographs of fracture surfaces of PPE/SAN blends following FCP testing. Crack growth rate of 10^{-4} mm/cycle. Crack growth parallel (a) and normal (b) to the injection-direction. The arrow indicated the direction of fatigue crack growth.

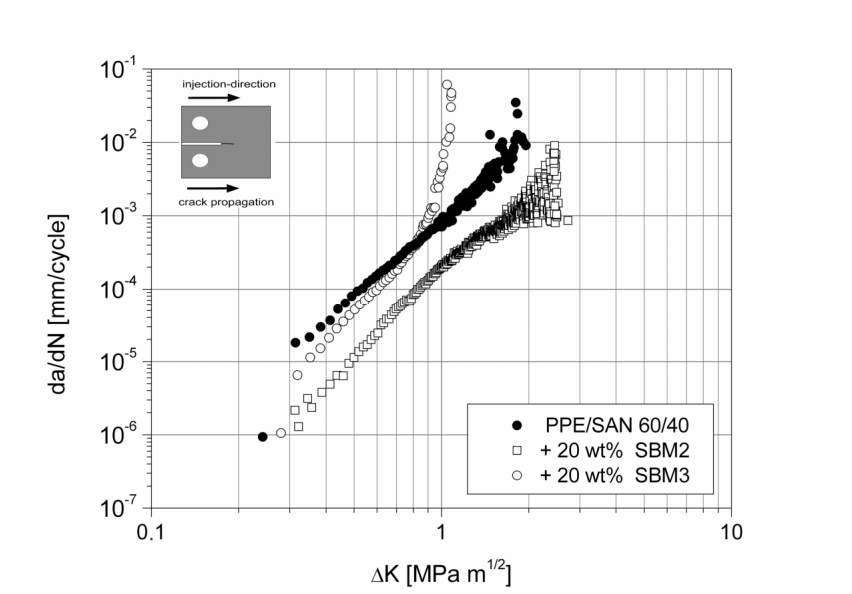

Figure 12: Influence of SBM compatibilisation on the fatigue crack growth behaviour of PPE/SAN blends. Open circles and open squares denote blends compatibilised by 20 wt% of SBM2 and SBM3, respectively. The uncompatibilised blend shown by the full circles is included for comparison. Crack growth was observed parallel to the injection-direction.

(a) PPE/SAN 60/40 + 20 wt% SBM2

(b) PPE/SAN 60/40 + 20 wt% SBM3

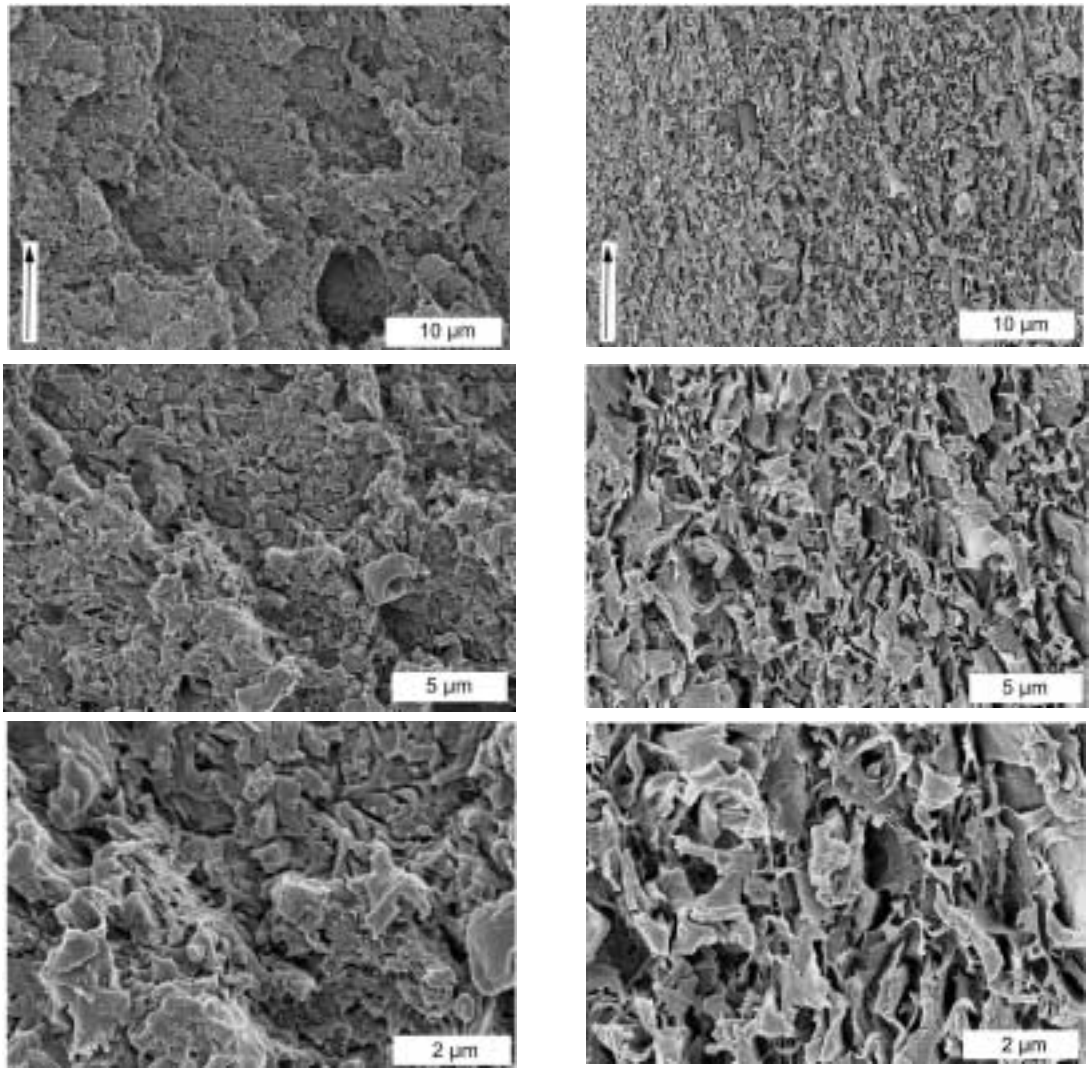

Figure 13: Representative SEM micrographs of fracture surfaces of compatibilised blends. Crack growth rate of 10^{-4} mm/cycle. PPE/SAN 60/40 blend compatibilised by 20 wt% of SBM2 (a) and SBM3 (b). The direction of crack growth is parallel to the injection-direction. The arrow indicated the direction of fatigue crack growth.

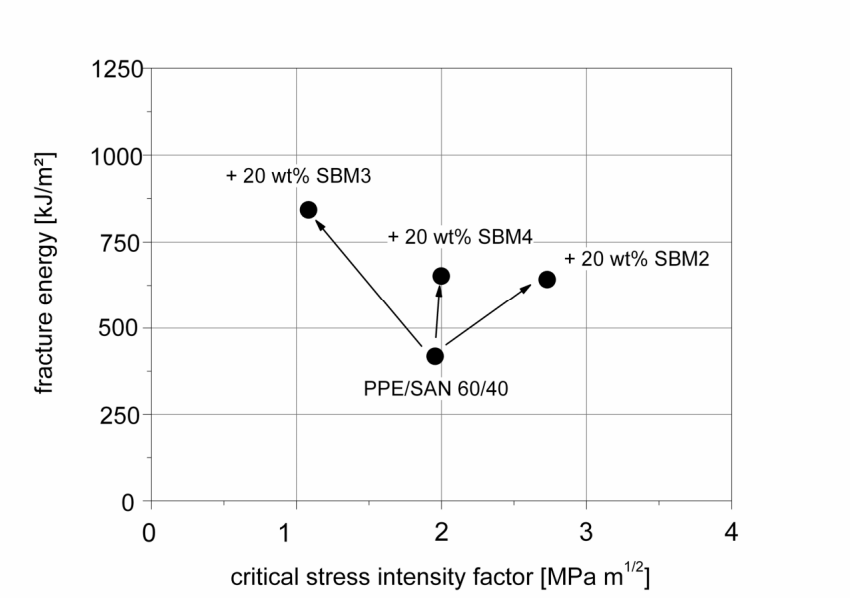

Figure 14: Summary overview of fracture energy (observed by tensile testing) versus critical stress intensity factor in parallel to the injection direction (observed by fatigue crack propagation) for the PPE/SAN 60/40 blend compatibilised by 20 wt% of the various SBM.